Summer 2018

Computational design and numerical analyses of thermal-hydraulics in a PWR-type small modular nuclear reactor

Vivek Murlidhar Rao

COMPUTATIONAL DESIGN AND NUMERICAL ANALYSES OF THERMAL-HYDRAULICS IN A PWR-TYPE SMALL MODULAR NUCLEAR REACTOR

by

VIVEK MURLIDHAR RAO

A DISSERTATION

Presented to the Faculty of the Graduate School of the

MISSOURI UNIVERSITY OF SCIENCE & TECHNOLOGY

In Partial Fulfillment of the Requirements for the Degree

DOCTOR OF PHILOSOPHY

in

CHEMICAL ENGINEERING

2018

Approved by

Dr. Joseph D. Smith, Advisor
Dr. Muthanna H. Al-Dahhan
Dr. Joontaek Park
Dr. Joshua P. Schlegel
Dr. Kelly O. Homan

PUBLICATION DISSERTATION OPTION

This dissertation consists of the following three articles, formatted in the style used by the Missouri University of Science & Technology:

Paper I: Pages 5-26 have been submitted to 'Nuclear Engineering and Design', an Elsevier publication.

Paper II: Pages 27-57 have been submitted to 'Annals of Nuclear Energy', an Elsevier publication.

Paper III: Pages 58-74 are intended for submission to 'International Journal of Heat and Mass Transfer', an Elsevier publication.

ABSTRACT

This dissertation focuses on computational design of a PWR-type small modular nuclear reactor (SMR), and analysis of coolant thermal-hydraulics during steady-state operation. Physical design of the SMR is based on the existing AP-1000 and Small Modular Reactor designs by Westinghouse Nuclear.

The first paper discusses a two-stage simulation of turbulent flow in the lower plenum of the RPV. In the first stage, four time-dependent Reynolds-Averaged Navier-Stokes (RANS) based turbulence models were used to simulate turbulent flow, compare predictions and identify an appropriate turbulence model. In the second stage, the selected turbulence model was once again used to simulate flow on a refined computational mesh (wall $y+ < 1$) and compared with time-averaged predictions of the Large Eddy Simulation (LES) model. The LES model was also able to capture a cut-off for the spatial frequency of inertial flow scales in the lower plenum.

The second paper uses simulation methodology established by Westinghouse Nuclear applied to resolving turbulent flow and heat transfer in a representative volume of the reactor core, as well as flow through the complex network of internal structures in the upper core. Predicted temperature profiles were in good agreement with design targets.

The third paper describes a two-stage study; the first compares predictions of RANS based models in resolving turbulent flow past the integral pressurizer, identifies the most suitable turbulence model, which is used in the second stage to simulate turbulent flow and heat transfer through both, pressurizer and steam generator units.

ACKNOWLEDGEMENTS

I am thankful to the Department of Chemical and Biochemical Engineering, Energy Research & Development Center at Missouri S&T, and Missouri Technological Corporation for financial support provided to the inception and completion of this work. I was at liberty to collaborate with colleagues in these departments, and I am grateful for the learning curve that emerged from these interactions. I am grateful to my committee members for their availability and willingness to discuss and learn, that greatly added to the scope of this project. I would like to thank our collaborators at Westinghouse Electric Company LLC, and the Small Modular Reactor Research and Education Consortium for tasking our group with a significant challenge, and an opportunity to transform a novel idea into a computational prototype. The outcome of this work will provide a template for future research in the field.

I would like to extend special gratitude to my adviser, mentor, and friend, Dr. Joseph Smith. I feel very fortunate to have been able to shadow his dynamism and independence while being extended ample opportunity to professionally grow and interact with industry. My colleagues who became wonderful friends – the long hours, laughs and get-togethers kept me going. I wholeheartedly wish them the best in their endeavors.

Without the moral support of my brother, parents, family, and dear friends, I would not be in this position. For unconditionally opening their hearts, minds, and homes to me, I am eternally thankful. This dissertation is dedicated to you.

TABLE OF CONTENTS

LIST OF ILLUSTRATIONS

PAPER I Page

PAPER II

PAPER III

LIST OF TABLES

NOMENCLATURE

PWR	Pressurized Water Reactor
SMR	Small Modular Nuclear Reactor
WSMR	Westinghouse Small Modular Reactor
MWe	Mega-Watt (Electric)
MWth	Mega-Watt (Thermal)
IRIS	International Reactor Innovative and Secure
CRDM	Control Rod Drive Mechanism
RCCA	Rod Cluster Control Assembly
TPA	Thimble Plug Assembly
RCP	Reactor Coolant Pump
RANS	Reynolds-Averaged Navier-Stokes
SST	Shear Stress Transport
RST	Reynolds Stress Transport

SECTION

1. INTRODUCTION

The availability of harnessed energy has become a necessity for social sustenance. Access to energy supply that is economically and logistically feasible, alleviates many socio-economic problems. Both, developed, and developing nations, have re-aligned focus towards energy security and resilience; delivering energy commodities under an umbrella of variability, as opposed to performance-based targets under normal circumstances [1]. The United States Department of Energy has advocated emphasis on research in renewable and hybrid energy systems. Harnessing energy from non-fossil sources is a potent step in reducing carbon dioxide and methane emissions, which in long-term objectives, is instrumental in mitigating the rise in global temperatures.

In reducing dependence on fossil fuel reserves and eventually replacing obsolete fossil fuel technologies, research in hybrid energy systems has gained traction. With grid power demand met by a cumulative supply from a primary fossil fuel energy generation source and numerous supplemental renewable energy sources, there is less demand from fossil energy sources, with increasing reliance on harnessing energy from renewable sources. In certain applications, the presence of auxiliary energy sources enhances the existing efficiency of systems generating energy from fossil fuels. Conceptual research and resilience strategies have shown that nuclear energy is a valuable component of such hybrid energy systems. Infrastructure for conventional nuclear power plants require access to secondary cooling systems, natural water sources, and an emergency protection zone, at minimum, which have a significant impact on the geographic vicinity. However,

a smaller production of nuclear energy bearing a fraction of the overall geographic footprint, would be more applicable as a reliable, secondary source of energy and power, meeting grid demand or supporting process industry with sensible heat for various applications. Some significant developments are discussed in the following sections.

1.1. MODULAR NUCLEAR ENERGY

Since design began in the early 2000s, the concept of making a 'module' of nuclear energy available for use has gained significant interest. By including many components of the primary circuit of the reactor inside the reactor pressure vessel, such a modular nuclear reactor is a competitor for small-scale energy generation (45-335 MWe). To utilities vendors and process industries, this is a logistic and economic feasibility. To reduce greenhouse gas (GHG) and carbon dioxide emissions, incorporating renewable energy systems such as solar/photovoltaics, wind and hydroelectric energy, has been the primary alternative. Permutations of renewable energy generation systems have been proposed where such small modular nuclear reactors (SMRs) are an advantage; a coupling of nuclear energy to the grid in terms of electricity production, sensible heat, or thermal storage for use by other systems [2]. However, known uncertainties in climatic conditions which these systems primarily rely on, adversely affect their reliability for on-line grid supply, and nuclear energy can play a critical role in meeting a potential deficit with innovative load-following capabilities of SMRs [3]. NuScale Power, LLC. published a study on the Horse Butte Wind Farm in Idaho, that analyzed the capability of an SMR in successfully offsetting the variability of electricity production from wind energy [4]. Further feasibility analysis of a nuclear-hybrid energy system has been conducted in the

western Texas and north-eastern Arizona regions [5]. The prospect of a nuclear-renewable energy system has been analyzed for several geographic locations in the USA [6]. Process modeling of a coal, wind, and nuclear hybrid energy system with real-time grid demand data has shown to provide a sustainable, reliable supply of electricity [7].

1.2. CURRENT SMR TECHNOLOGIES

Historically, there have been several nuclear fuel technologies in use in industry. Solid UO2 fuel cooled by pressurized light-water; molten salt fuel moving through a reactor with graphite moderator to control the reaction and heat removal; and high temperature gas cooled breeder reactors have been the most commonly adopted technologies. Each technology has presented a comprehensive learning curve with operational issues, on which several SMRs have been conceptualized. In the USA, NuScale Power LLC is presently in the process of securing a license from the United States Nuclear Regulatory Commission, for their pressurized light-water cooled SMR, designed to generate 45 MWe [8]. Other notable participants in the SMR movement include Westinghouse Electric Company, LLC, with a PWR SMR design rated at 225 MWe; and a collaboration between GE Hitachi Nuclear Energy and Advanced Reactor Concepts, LLC, for the ARC-100 100 MWe design, a sodium cooled ‘fast-neutron-spectrum’ reactor [9, 10]. In 2010, AREVA Inc. proposed a high-temperature gas cooled SMR, the SC-HTGR – a Generation IV SMR, which was approved by the Next Generation Nuclear Plant (NGNP) group for commercialization of HTGR technology, while X Energy, LLC have developed the Xe-100 series HTGR SMR [11, 12]. In molten salt reactors, Terrestrial Energy have brought forward the integral molten salt reactor

(IMSR) SMR that can produce up to 190 MWe, using molten fluoride salt to transport nuclear fuel in the reactor [13].

1.3. OBJECTIVE

This dissertation focuses on light-water cooled, nuclear fission reactor technology, and is based on the SMR design by Westinghouse Electric Company, LLC, namely the WSMR. The addition of a hot leg riser and integral pressurizer unit presents a new flow path compared to conventional PWR designs, which mandates a thorough analysis of thermal and hydrodynamic profiles. Significance is given to (i) resolution of turbulent flow structures using time-dependent formulations of equations describing momentum transport and turbulent parameters (ii) conjugate heat transfer in a representative volume of the reactor core, and (iii) capturing underlying phenomena in flow of the primary coolant past the integral pressurizer into the integral once-through steam generator, while also quantifying heat transfer to the shell side of the steam generator in terms of outflow steam quality (design metric).

PAPER

I. SIMULATION OF TURBULENT FLOW IN THE LOWER PLENUM OF A PWR-TYPE SMALL MODULAR NUCLEAR REACTOR

ABSTRACT

Turbulent flow in the lower plenum of a pressurized-water small modular nuclear reactor was simulated using commercial CFD package, STAR-CCM+, to compare the performance of different RANS based turbulence models with a transient formulation. The study was conducted in two phases: (i) a preliminary study with RANS-based models in transient formulations - the Realizable k-ε Model, SST k-ω Model, Reynolds Stress Model, and Spalart-Allmaras Model. Turbulent flow was simulated with each model for 10 residence times, and hydrodynamic data from the simulations were compared. The time-averaged profiles of velocity magnitude in the lower plenum indicated lateral flow non-uniformity, which was inferred as the presence of recirculation zones and possible transient flow phenomena. The coefficient of variation was calculated based on the velocity profiles, with the lowest value reported by the Reynolds Stress Model. Accordingly, the mesh from phase (i) was refined such that wall $y^+ < 1$ on which phase (ii) of the study was conducted. This phase focused on comparing hydrodynamic predictions from the Reynolds Stress Model and time-averaged values from the Large Eddy Simulation Model. Additionally, a power density spectrum of turbulent kinetic energy calculated for eddies from the Large Eddy Simulation Model was able to capture the spatial frequency corresponding to the inertial sub-range, and a cut-off frequency, beyond which viscous forces are dominant. Accordingly, the results from phase (ii) were taken with statistical confidence.

1. INTRODUCTION

Small modular nuclear reactors (SMRs) are designed to provide nuclear energy to process industries and utilities. A primary motive for SMR deployment is to support and eventually replace fossil energy production or provide power supply in hybrid energy and microgrid systems [1]. The smaller size requires less time for construction, and is a logistic convenience, allowing on-site assembly. Modularity is achieved by integrating primary circuit components that are conventionally located outside the reactor pressure vessel (RPV); namely, the pressurizer, steam generator(s), and reactor coolant pumps (RCPs). One of the first pressurized light water SMR designs – International Reactor Innovative and Secure (IRIS - 330 MWe), translated this modular concept into design. SMRs have been based on existing PWR or HTGR technology; however, molten salt reactors (MSRs) are gaining attention due to less complexity with refueling operations, and higher heat removal capacity at atmospheric pressure. The main objective of this study is to provide a thorough, skeletal analysis for thermal hydraulics in SMRs, that can be applied to different SMR technologies. The 225 MWe SMR design by Westinghouse Electric Company LLC (WSMR), was used as a basis for this study.

Compared to the AP1000, the WSMR requires lower capital costs, and provides enhanced passive safety features that meet regulations for nuclear non-proliferation, creates a lower carbon footprint, and affords power to utilities at lower costs [2]. The use of a WSMR to potentially support a hybrid – coal, wind, and nuclear energy system was explored, and was shown to create a sustainable supply for power grids [3].

In terms of physical design, the WSMR uses fuel rods with a shorter active length (8 ft. vs. 12 ft.), fewer fuel assemblies (89 vs 192) and a lower core thermal output (800MW vs. 3400 MW), which require less coolant flow from the reactor coolant pumps (RCPs) (100,000 gal/min across 8 RCPs, vs. 400,000 gal/min across 4 RCPs). Other salient comparisons are provided in Table 1.

Table 1. A general comparison of WSMR and AP1000 features [3].

	Site Area (acres)	Reactor Coolant Loop Piping	Control Rod Drive Mechanisms	Rail/Truck/ Barge Shipment
WSMR	15	No	Inside RPV	Yes
AP-1000	100	Yes	Outside RPV	No

2. SIGNIFICANCE

The lower head of the RPV and lower plenum contain support structures which direct coolant flow into the reactor. Prior to analysis, design considerations must arise from past performance of structures and their integrity. Of importance, are generally, loss of coolant accidents(LOCA) which could lead to a meltdown of the reactor core. Bottom nozzles of fuel assemblies are fitted with debris filters to restrict transport of this material. However, during a LOCA accident, the fuel temperature can exceed design limits of materials, and allow debris to enter the lower plenum. Several studies have focused on the integrity of the lower head, and safe retention of the core debris during re-flooding of the reactor core for primary heat removal. A Risk-Oriented Accident Analysis Methodology (ROAAM) was applied to the Westinghouse AP600 and Westinghouse

AP1000 to evaluate the heat removal capacity of the lower head during core melt and test the thermal and structural limits during heat removal from the exterior wall by the containment [5-6]. To prevent high pressure core damage, situations such as high-pressure melt ejection (HPME) were considered, to restrict the transport of debris to the lower head by providing auxiliary heat removal and depressurization. Similarly, the impact of multi-layer corium formation was assessed on the structure of the RPV [7]. In 2015, Westinghouse Electric Company presented design cases for the AP1000 that allow for long term containment of core melt, with ultimate venting of the containment structure, mitigating debris release, including quenching of core debris on the lower head of the RPV by incoming coolant flow [8]. However, little work has been published in thermal hydraulics on the flow behavior in the lower plenum of the AP1000. While the WSMR design is based on the AP1000, it is important to analyze thermal-hydraulic behavior in detail and incorporate relevant improvements from the AP1000 design into the current study. Focus on true geometry modeling, without approximations such as porous media, have provided improvements in existing design [9].

The use of computational fluid dynamics (CFD) has been well studied in nuclear technology. Much work has been published in CFD modeling of lower plena for high-temperature, gas-cooled reactors (HTGRs). Lower plena in HTGRs generally experience a greater hydraulic load, directly receiving coolant flow from the RCPs, before a 90^0 re-direction into a prismatic core. The use of commercial CFD package, FLUENT 6.2.16 was assessed against data from Matched-Index-of-Refraction (MIR) for very-high temperature reactor (VHTR) tests at Idaho National Laboratory [10]. Large eddy simulation (LES) modeling of flows in a VHTR was conducted to show the importance

of reactor-wide modeling, compared to a $1/8^{th}$ section of the reactor, where the influence of inertial agitation on temperature in the center of the upper plenum was not replicated [11]. In a collaborative effort between the USNRC and the Czech Technical University (CTU) to support HTGR licensing, various air ingress conditions were studied in the lower plenum of an HTGR where convection is driven by natural circulation and molecular diffusion [12]. A massively parallel CFD code, FUEGO, developed at Sandia National Laboratory, was used to conduct an LES calculation that resolved inlet flow dynamics – vortices, internal recirculation and stagnation zones, high and low mixing zones – to study hot spot formation (up to 200 K higher than average), and provide an understanding of flow patterns past complex geometries in NGNP gas-cooled reactors [13]. A considerable number of experimental studies have been conducted in conjunction with CFD modeling, for plena dynamics in NGNP Gas-cooled reactors, and VHTR CFD assessment [14-15]. This paper presents the computational analysis of turbulent flow in the downcomer of the RPV, past internal structures in the lower plenum of the WSMR, and outflow into the reactor core. Available dimensions in the Westinghouse Technology Systems Manual for PWRs were used to design the computational model in the current study [16].

3. FLOW PHYSICS

3.1. LOWER PLENUM FLOW PATH

The lower plenum is comprised of a downcomer formed below the 8 RCP discharge side inlets, and between the core barrel and the RPV wall, there are 4 neutron

shield pads, the core barrel, the lower core support plate, the lower core plate, support columns and a secondary support structure. RCP discharge flow impinges against the core barrel wall and descends the downcomer. Flow exiting the downcomer is obstructed by the sole plate at the bottom and the secondary support structure. A vortex suppressor plate is included in this study; the plate reduces area normal to core inflow, prior to the lower support plate, and is expected to channel flow into the lower support plate. The lower support plate is connected to the secondary support structure via support columns. While the lower support plate primarily serves a structural role, it also straightens flow directed to the reactor core. The core inflow is further directed to the fuel assemblies through the lower core plate, with 4 holes per fuel assembly. The reactor core includes 89 fuel assemblies.

Large internal structures such as support columns, plates, and neutron shield pads non-uniformly alter the available flow area and are expected to affect the flow field which may not be theoretically predicted. A key objective of this work was to compare turbulence models that can analyze flow in these regions and identify flow patterns that require validation. Figure 1 shows a schematic of the flow path (green outline) considered in this study - from the RCPs to the lower core plate, with an elevation view of the CAD model.

3.2. OPERATING CONDITIONS, ASSUMPTIONS, AND SIMULATION SETUP

The study-wide operating conditions, and thermophysical properties of the coolant are listed in Table 2.

Table 2. Operating conditions for simulation setup.

Operating Pressure (Pa)	RCP Flow Rate (gal/min)	Inlet Temperature (K)	Density (kg/m^3)	Viscosity (kg/m-s)
15411878.25	100,000	564	744.46	9.2062E-5

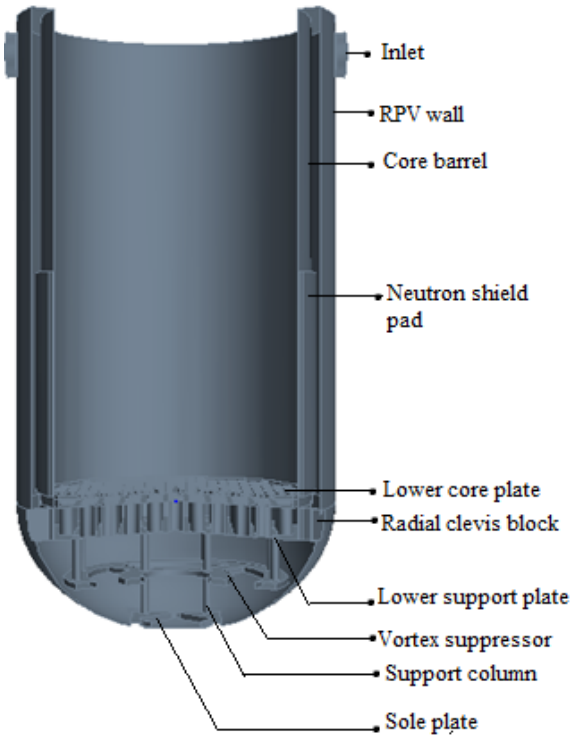

Figure 1. Sectional elevation view of the WSMR CAD model.

i. Since the RCPs are not a part of this study, the thermal effects of flow through the pump cannot be considered. Also, it has been assumed that such effects on thermophysical fluid properties are insigfnificant when compared to the changes induced by heat transfer in the reactor core. Thereby, the flow may be considered isothermal.

ii. It is assumed that flow in the SMR design is initially static. All dynamic effects are introduced only at the start of the simulation. Backflow from the reactor core

is not considered. The goal of each simulation study is to predict the performance of the corresponding turbulence model in predicted turbulent flow during steady-state operation. Under this purview, the ability of each turbulence model to resolve the transient nature of turbulent flow and associated effects is studied using transient formulations of the Reynolds Averaged Navier Stokes equations, in STAR-CCM+.The preliminary computational grid consisted of 10,451,843 hexahedral cells. The discharge side of the RCPs were set as the domain inlet, and the holes in the lower core plate, as the outlet. Figure 2 shows the level of mesh detail used for phase (i) of the study.

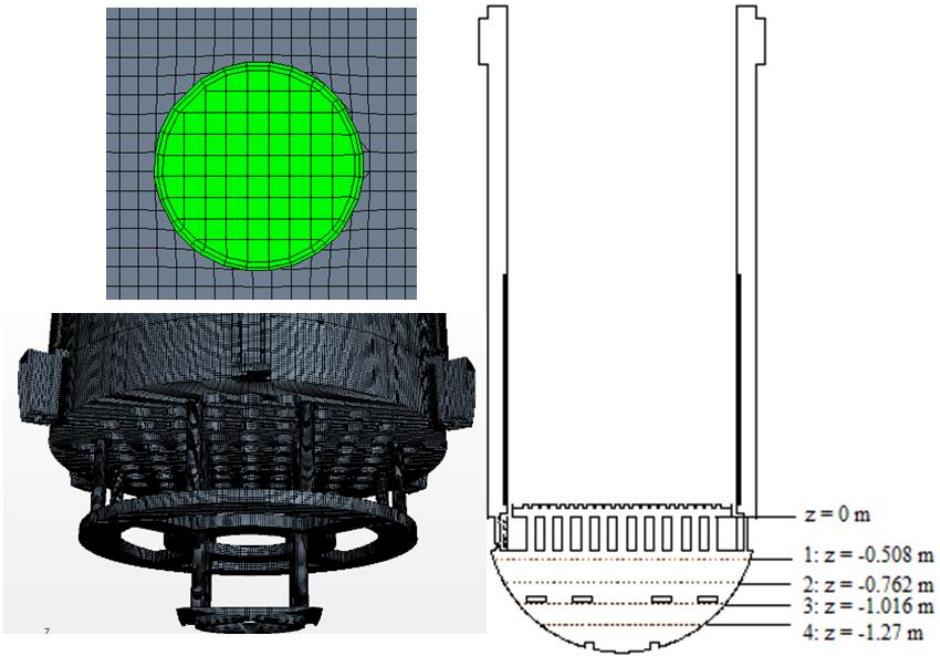

Figure 2. (a) Mesh detail on 1 of 366 domain outlets on the lower core plate (b) mesh detail on internal structures in the lower plenum (c) sampling locations set up in the lower plenum.

4. SIMULATION, RESULTS, AND DISCUSSION

4.1. PHASE I – PRELIMINARY ANALYSIS OF TURBULENT FLOW PREDICTIONS

When simulating flow through complex, symmetric geometries, an important check is to test for hydrodynamic symmetry about the domain axes. In this study, the plenum volume below the lower support plate and the annular downcomer is of primary interest. To assess symmetry within this volume, time-averaged velocity profiles were compared at the locations indicated in Figure 2 (c). The lateral variation in velocity magnitude at four linear probes, is presented in Figure 3.

At z = -1.27 m, the axial component of flow exiting the downcomer is subjected to wall curvature and thus, wall effects, which are manifested as sharp changes in velocity magnitude near x = +/- 1.5 m. While all four models are accompanied by the y+ wall treatment model to model wall effects, it is evident that steep veloicty gradients between adjacent cell layers in the near-wall region arise due to a lack of resolution in the boundary layer. Accordingly, the cell layers adjacent to the near-wall region which are not subjected to wall y^+ treatment receive flow with kinetic energy parameters not calculated as accurately as may be predicted. This can be observed as an abrupt increase in velocity magnitude away from the near-wall region. Below in Table 3, a comparison of the coefficient of variation (CoV) based on velocity profiles reported by the four simulations is provided.

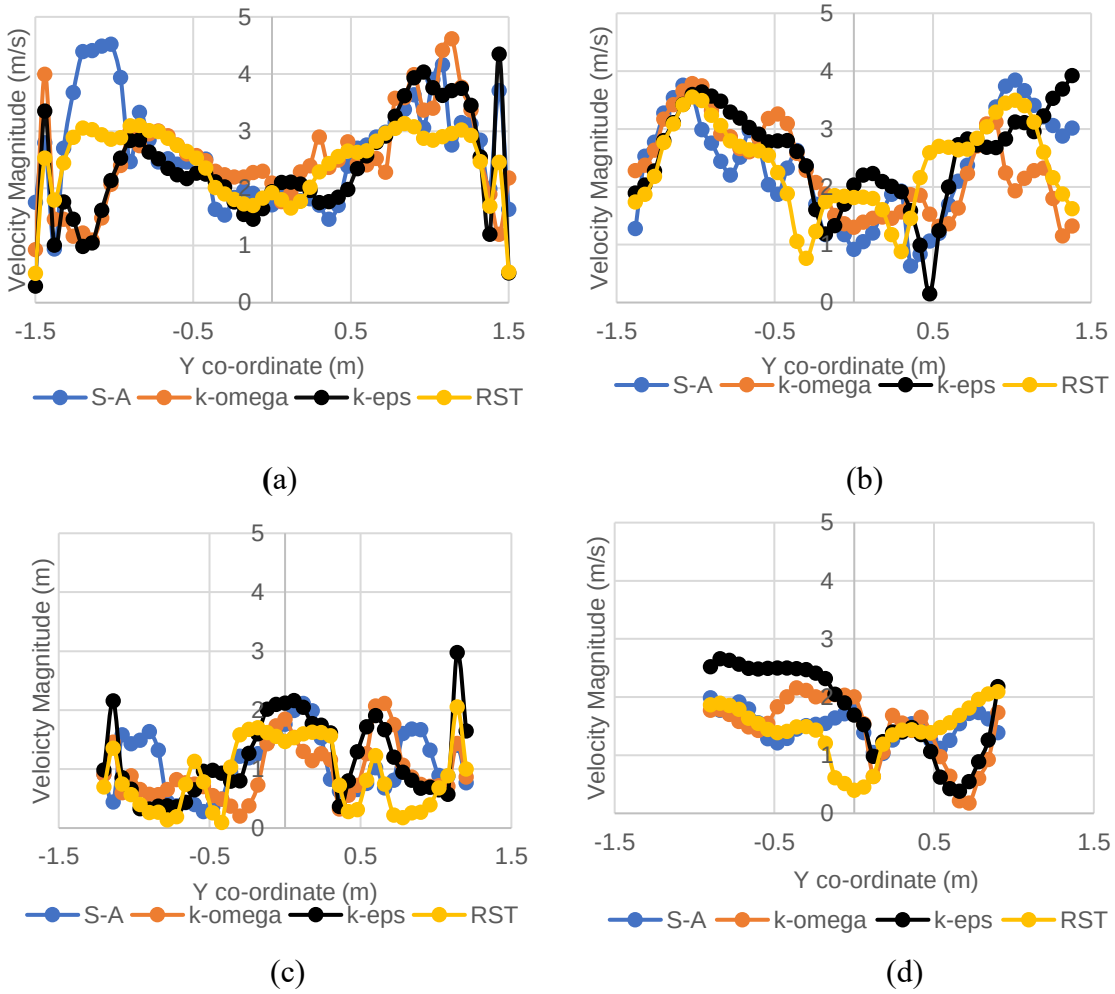

Figure 3. Lateral variations in time-averaged velocity magnitude at elevations below the lower core plate: (a) z = -1.27 m (b) z = -1.016 m (c) z = -0.762 m and (d) z = -0.508 m.

Table 3. Statistical analysis of predicted velocity profiles.

Coefficient of Variation	Spalart-Allmaras	k-epsilon	k-omega	RST
z = -1.27 m	0.33977	0.39738	0.33314	**0.25181**
z = -1.016 m	0.38896	**0.32088**	0.33070	0.320961
z = -0.762 m	**0.47282**	0.56781	0.50415	0.65444
z = -0.508 m	**0.16591**	0.42375	0.37843	0.32592

As the sampling locations ascend into the interior flow at z = -1.016 m, -0.762 m, -0.508 m, it is observed that larger variations in time-averaged velocity magnitude exist near the center of the sampling locations, which aligns with the axial center of the lower plenum. While this behaviour is predicted by all four models, the RST model provides the most gradual and relatively symmetric change in predictions for both, interior, and near-wall flows. This may be attributed to the direct calculation of all stresses by the RST model formulation. The contribution of additional stresses in the RST simulation of flows emerging from the turbulent boundary layer provides a more accurate mean flow representation than those reported by the other RANS simulations. From Table 3, it may be inferred that the S-A model provides lower CoV values than the other turbulence models for z = -0.508 m and z = -0.762 m. However, the S-A model has been proven to not capture rapid changes in turbulent length scale with a one-equation formulation, and in this case, it is suggested that the S-A model does not resolve boundary-layer flows with the accuracy of the RST model [17]. Additionally, fluid exiting the downcomer faces a non-uniform increase in available flow area but is obstructed by the vortex suppressor plate and support columns prior to flowing past the lower support plate into the lower core plate. This introduces the possiblity of rotational flow and vortex shedding in the lower plenum which must be investigated. Consequently, phase (ii) of the study was conducted on a mesh with $y^+<1$.

4.2. PHASE II – MESH REFINEMENT AND LARGE EDDY SIMULATION (LES) STUDY

Based on the preliminary simulation results, it was observed that flow in the downcomer is subjected to flow past six neutron shield pads which are significant in

length compared to the length of the downcomer. The presence of sharp edges introduces the possibility of flow separation and re-attachment phenomena. While the inlet flows are driven by the RCPs, the descent of flow in the downcomer is initially driven by angular momentum and later, predominately aligned with the gravitational vector. This is necessary in determining the use of a structured or unstructured grid for the volume mesh. For the downcomer volume, a polyhedral mesh was chosen as the volumetric mesh model because polyhedral cells can better conform to curved edges in the geometry, as well as thin edges when local size refinement is considered. It is essential to capture gradients in the initial flow of the dowcomer with a refined mesh, as the effect of body forces on flow entering the downcomer is further subjected to boundary layer – wall y^+ treatment in the lower plenum volume. A refined polyhedral mesh in the downcomer volume is suggested to accommodate for an accurate capture of developing flow phenomena.

However, in the lower plenum volume, the flows are seen to develop significant lateral gradients due to the flow reversal induced by the 180^0 dome-like curvature of the plenum. In this volume, developing flow is aligned with the reactor axis by the lower support plate and passed through the lower core plate which directly aligns with the fuel assemblies. Hence, it is critical to solve for flow profiles on a computational grid aligned with the reactor geometry. Thus, a hexahedral/cut-cell volumetric mesher was chosen for this volume. The mesh settings used to generate a wall $y^+<1$ are listed in Table 4. Figure 4 shows the mesh detail in both volumes, on the outlet surfaces, and at the walls of internal structures in the lower plenum volume.

Table 4. Mesh settings for phase (ii) of the study.

Domain	Downcomer Volume – Polyhedral Mesh		Lower Plenum Volume – Hexahedral Mesh			
Parameter	Minimum Surface Size	Target Surface Size	Minimum Surface Size	Target Surface Size	No. of Prism Layers	Prism Layer Total Thickness
Value	0.00025 m	0.0025 m	0.0004 m	0.004 m	2	0.001 m

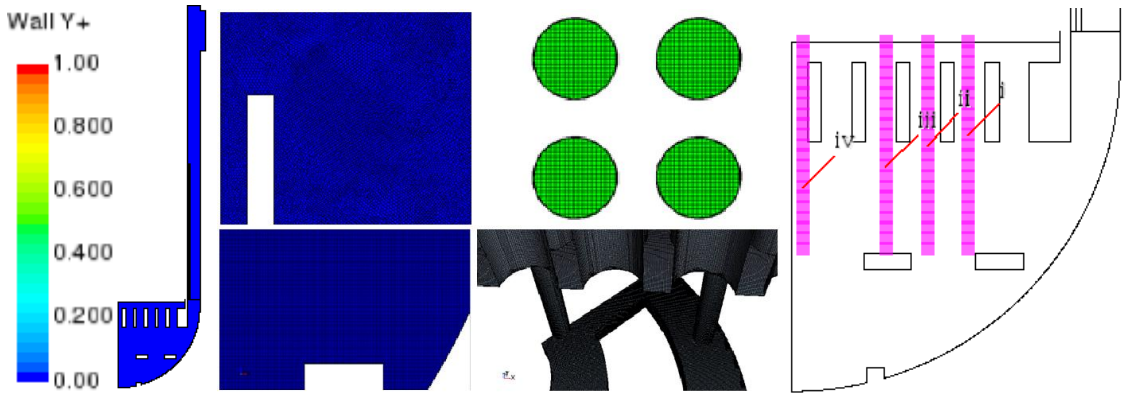

(a) (b) (c)

Figure 4. (a) Scalar contour of wall y+ (b) mesh detail on downcomer face (L-top) and lower plenum face (L-bottom); mesh detail at outlets of the lower core plate (R-top) and at support structure walls (R-bottom) (c) locations of linear sampling probes in the lower plenum.

As listed in Table 4, the size settings are about three orders of magnitude smaller than the reactor dimensions. To reduce the number of cells, a 60^0 section of the preliminary model was considered. This section was selected such that all the geometric features and internal structures found inside would form a repetitive pattern in the 360^0 model. Symmetry faces were created where required. The computational grid on this 60^0 model consisted of 94,837,981 cells with a minimum face validity of 0.95. On this mesh,

two simulations were executed with a time step of 1e-5 s, for ten residence times (24 s) – one simulation with the RST model, and one simulation with the LES model. Figure 5 compares time-averaged velocity profiles between the RST model and LES model predictions after ten residence times. As may be inferred from Figure 5, there is a significant impact of turbulent fluctuations on the interior flow which is not captured by the RANS-based RST model, due to the inherent temporal averaging in the numerical formulation. On the other hand, the LES model solves for near-wall flows as well as interior flows, without damping the fluctuating component of velocity. The difference in time-averaged profiles reveals the effect of damping the fluctuating component of velocity by RST model, as opposed to the higher time-averaged profile predicted by the LES model.

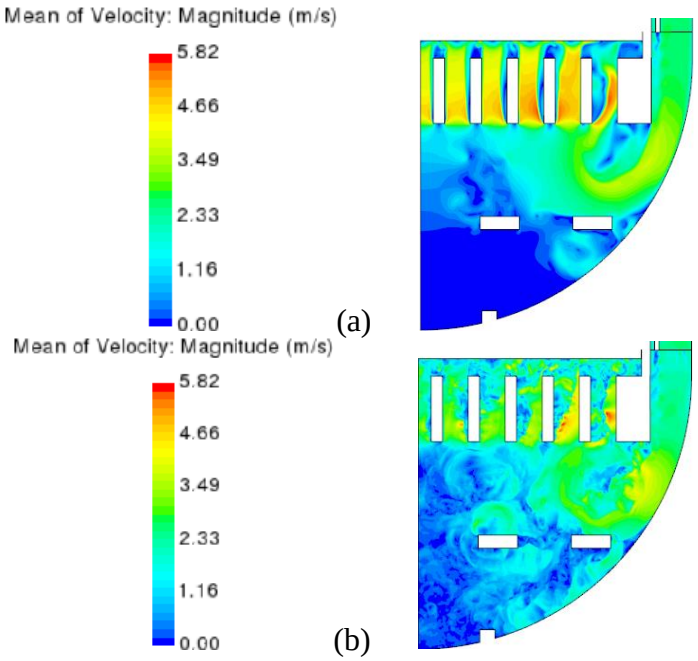

Figure 5. Time-averaged profiles of velocity magnitude predicted by (a) RST and (b) LES models.

The LES model uses a filtering of flow scales above a computed threshold for the turbulent length scale, above which, all 'large' eddies are solved for, while the smaller eddies are treated with a sub-grid scale model; the Smagorinsky Sub-Grid Scale (SGS) model in this case, where viscous stresses are dominant and energy dissipation is driven by diffusive forces. Accordingly, it is essential to quantify the proportion of the solution that is rendered to the SGS model, so that the need for mesh refinement can be assessed in the corresponding cell vicinity. For this, a function 'ratio' was defined using the large-eddy turbulent kinetic energy (k_{les}) and the SGS model-treated turbulent kinetic energy (k_{sgs}) [19].

$$ratio = \frac{k_{les}}{(k_{les} + k_{sgs})}$$

This function was plotted across an axial cross-section plane in the downcomer and lower plenum volumes, in Figure 6 (a). From Figure 5 and Figure 6, it is observed that the time-averaged velocity profile in the lower plenum is largely solved by the LES model, where damping effects are minimal. Further, a comparison of the time-averaged turbulent kinetic energy reported for non near-wall flows by the RST model, and large-eddy scale flow by the LES model shows a fundamental difference in the model predictions – the inherent temporal averaging of the RST model mitigates the contribution of fluctuating velocity components to flow rising from the lower plenum into the lower support plate, while the LES model is able to identify relatively smaller flow structures in the large-eddy regime of turbulent flow and predict local perturbations in flow rising through the plenum.

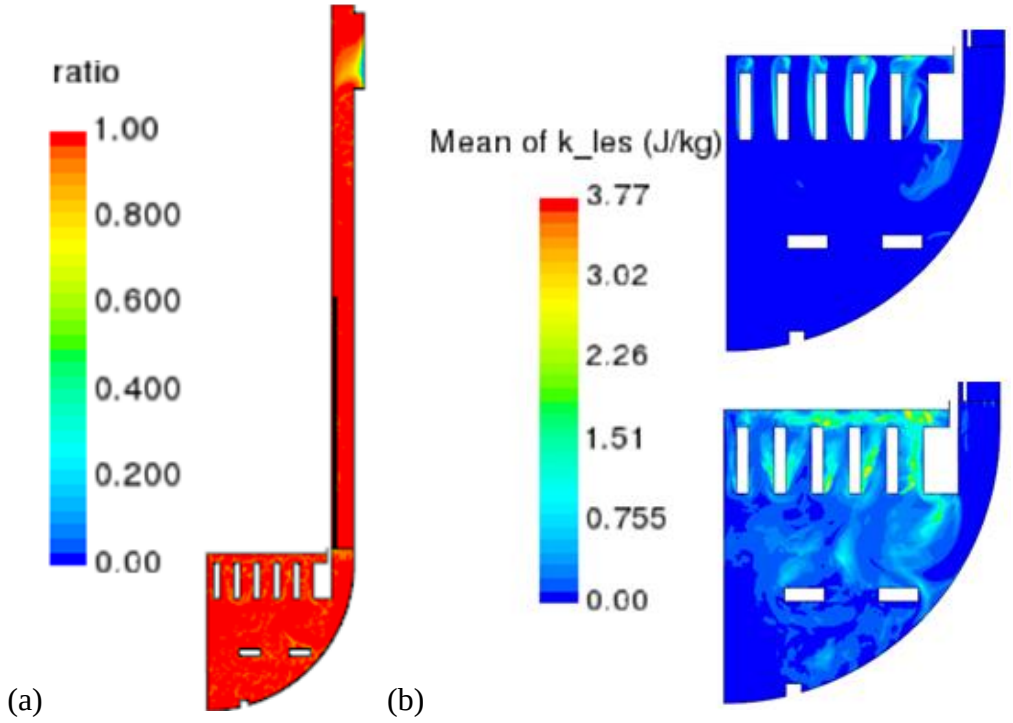

Figure 6. Scalar contours of (a) ratio of solution explicitly calculated for large scales of energy to total energy resolution and (b) turbulent kinetic energy reported by RST model (top) and LES model (bottom).

These perturbations also anchor re-attachment sites at the hole edges of the lower support plate, which in turn indicate lateral dispersion of flow rising through the lower support plate. In comparison, the RST model predicts dominant near-wall flows through the lower support plate, which appear to swirl at the upper surface of the lower support plate. This phenomenon is predicted as a relatively dispersed profile by the LES model. Flow rising into the lower support plate primarily originates from bulk flow in the lower plenum. The lower support plate serves as a flow straightener and enhances the axial component of flow to provide uniformity for reactor core inflow. Time-averaged axial velocity profiles predicted by LES and RST models are compared in Figure 7.

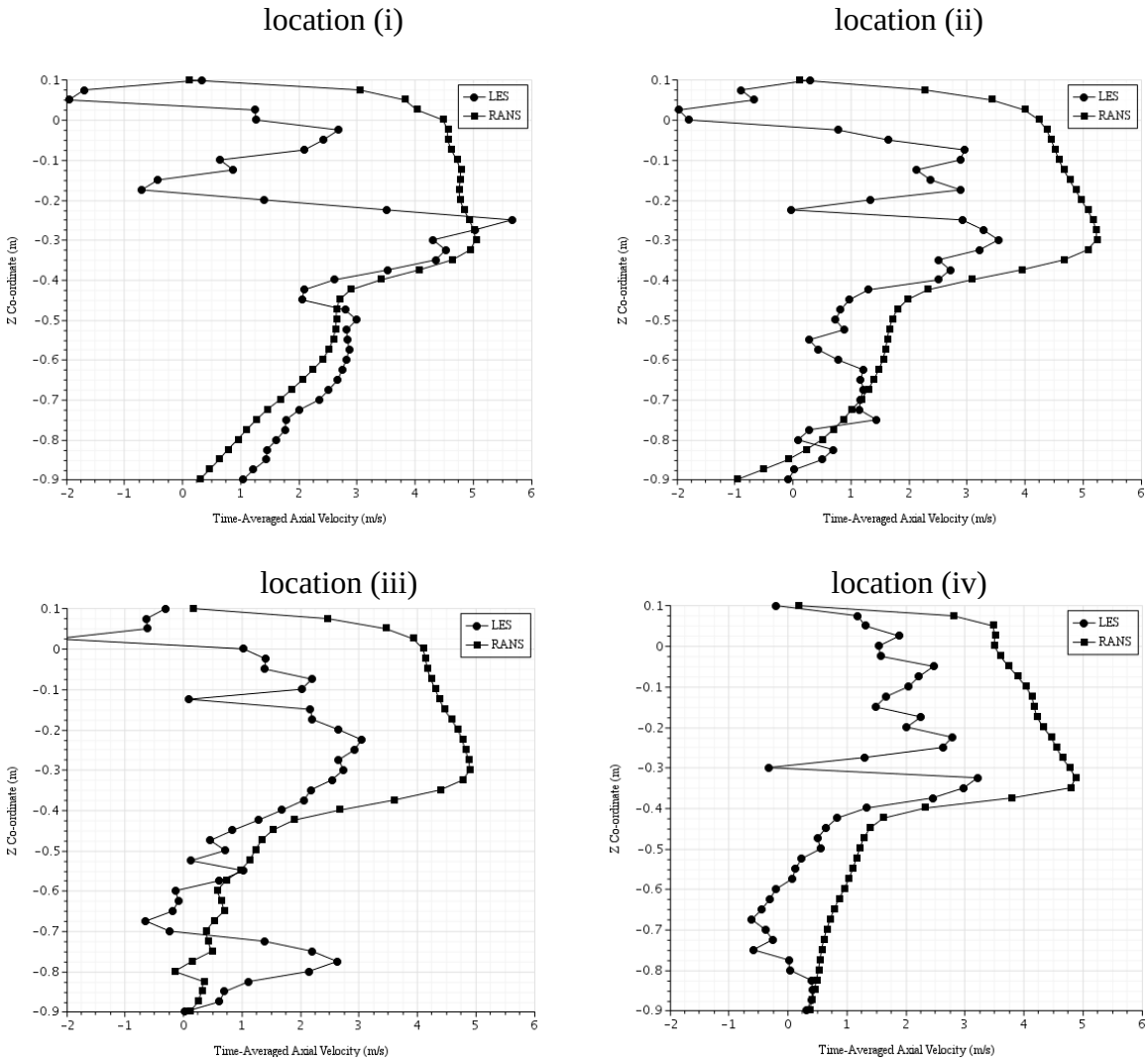

Figure 7. Profiles of time-averaged axial velocity at the four linear sampling probes (indicated in Figure 4 (c)) in the lower plenum.

As indicated in Figure 6 (b), higher energy flow is anchored at the base of the downcomer proximal to the lower support plate. With near-wall flows descending along the curved walls of the lower plenum, the higher energy flow is not provided with a sufficient volume, directing a portion of the flow into the closest holes of the lower support plate. This effect may be observed in Figure 7 (a) and Figure 7 (b). Relatively, the interior flows are observed to possess less turbulent kinetic energy and pass through

the lower support plate with less perturbation in the axial component of velocity. This reduces towards the center of the lower plenum volume and may be observed in Figure 7 (c) and Figure 7 (d).

To test the sufficiency of mesh refinement, a point probe was placed in the lower plenum and samples of turbulent kinetic energy were collected. A 'Data Set Function' was created with this sampling monitor in STAR-CCM+, upon which a power density spectrum of turbulent kinetic energy was obtained, as shown in Figure 8.

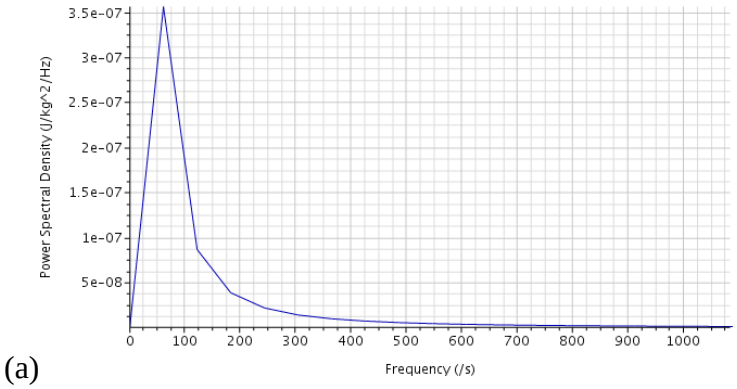

(a)

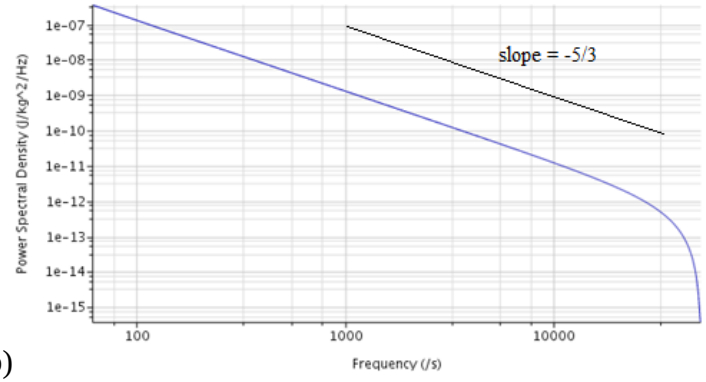

(b)

Figure 8. (a) Power spectral density of turbulent kinetic energy (b) a log-log plot of data from (a) obtained on the mesh containing 95M cells.

From turbulence theory, it has been shown that in the inertial sub-range, the kinetic energy of turbulent structures is proportional to the (-5/3) power of the spatial frequency of large eddies [20]. In Figure 8, a representative line with a slope of (-5/3) is provided for comparison. The spectra suggest that the LES predictions are satisfactorily in the inertial sub-range and predictions from the LES model may be taken with satisfactory confidence for further investigation.

5. CONCLUSIONS

Different turbulent models available in STAR-CCM+ were studied in two phases to analyze turbulent flow in the downcomer and lower plenum of a SMR based on the WSMR design. Turbulent flow was resolved in the preliminary calculations using the Realizable k-ε model, SST k-ω model, RST model, and the Spalart-Allmaras model – all based on an unsteady RANS formulation. Due to averaging at each time step, the turbulent fluctuations were damped, resulting in smooth profiles at the sampling locations, except for the RST model, which consistently predicted span-wise undulations in velocity profiles, indicative of transient flow phenomena. This was attributed to the additional stress terms solved only by the RST model, at a higher computational cost. Hence, the RST model was selected for the second phase of the study.

In the second phase of the study, the RST model and LES model were used to simulate turbulent flow. After the initial flow developed, the simulations were run for ten residence times each, and the time-averaged profiles were compared. Due to the inherent averaging process of the RST model formulation, turbulent fluctuations are damped at

each time step, affecting the contribution of dominant components to the bulk flow. The LES model was able to predict a larger volume of high energy flow in the lower plenum, which in comparison with the RST model, was significant as the extent of lateral dispersion affects the contribution of axial velocity in flow rising through the lower support plate. This was manifested by backflow indicated by the LES model predictions for flow through holes of the lower support plate closer to the downcomer, and more qualitative agreement with RST predictions at the sampling locations closer to the center of the lower plenum volume.

Lastly, turbulent kinetic energy of large scale flows was sampled to check if further mesh refinement was required for simulation with the LES model. As a check, the power density spectrum of turbulent kinetic energy was plotted based on large-eddy turbulent kinetic energy data sampled at a point in the lower plenum where flow separation was observed, and the obtained spectrum provided qualitative agreement with the expected energy cascade, followed by a sharp cut-off, indicating a successful resolution of flow scales in the inertial sub-range of turbulent flow.

ACKNOWLEDGEMENT

The authors would like to thank Westinghouse Electric Company, LLC, for guidance in the CFD study. The authors are grateful to Missouri Technology Corporation (MOTEC), the Small Modular Reactor Research and Education Consortium (SMRREC) at Missouri University of Science & Technology, and the Department of Chemical and Biochemical Engineering for funds and computational resources provided towards

research efforts. Lastly, the authors are grateful for access to computational resources at Oak Ridge Computing Facility, Oak Ridge National Laboratory, without which phase (ii) of the study would not have been possible.

REFERENCES

1. Bragg-Sitton, S. 2015. Handbook of Small Modular Nuclear Reactors. 13 – Hybrid energy systems (HESs) using small modular reactors (SMRs). Woodhead Publishing, ISBN 978-0-85709-853-5.

2. Westinghouse Electric Company, LLC. http://www.westinghousenuclear.com/New-Plants/Small-Modular-Reactor. (accessed: August 16, 2017)

3. Buchheit, K.L.; Smith, J. D.; Guntupalli, U.; Chen, C.; 2016. Techno-Economic Analysis of a Sustainable Coal, Wind, and Nuclear Hybrid Energy System. Energy Fuels. 30 (12), pp 10721-10729.

4. Collado, J. M. Design of the Reactor Pressure Vessel and Internals of the IRIS Integrated Nuclear System. United States Nuclear Regulatory Commission. Accession Number: ML033600078. https://www.nrc.gov/docs/ML0336/ML033600078.pdf (accessed: 03/23/2018)

5. United States Nuclear Regulatory Commission. Westinghouse AP 1000 Design Control Document Rev. 19. Accession Number: ML11171A500. Date Released: Tuesday, June 21, 2011.

6. Sanchez, J. I.; Lage, C. A.; Nunez, T.; 2001. LBLOCA Analysis in a Westinghouse PWR 3-Loop Design Using RELAP5/MOD3. United States Nuclear Regulatory Commission. Date Published: January 2001.

7. Kim, T. H.; Kim, S. H.; Chang, Y-S.; 2015. Structural Assessment of Reactor Pressure Vessel Under Multi-Layered Corium Formation Conditions. Nuclear Engineering and Technology 47 (3), pp. 351-361.

8. Taylor, J., 2015. Long Term Containment Protection Strategies for the AP 1000 © Plant Design. Westinghouse Electric Company LLC. Date published: September 2015.

9. Jeong, J. H. and Han, B-S. 2008. Coolant flow field in a real geometry of PWR downcomer and lower plenum. Annals of Nuclear Energy, 35, pp. 610-619.

10. Guillen, D. P. 2006. Computational Flow Predictions for the Lower Plenum of a High-Temperature, Gas-Cooled Reactor. Publication Number: INL/EXT-06-11780.

11. Uribe, J.; Moulinec, C.; Rabbitt, M.; Howard, R.; Emerson, D. R.; 2013. LES of the Flow inside the Lower Plenum of an Advanced Gas-Cooled Reactor with Conjugate Heat Transfer. Procedia Engineering, 61, pp. 192-197.

12. Gregor, K. and Dostal, V. 2011. CFD simulations of separate effects in an HTGR lower plenum under air ingress condition. Nuclear Engineering and Design, 251, pp. 407-411.

13. Rodriguez, S. B.; Domino, S.; El-Genk, M.S.; 2010. Safety Analysis of the NGNP Lower Plenum Using the FUEGO Code. Computational Fluid Dynamics (CFD) for Nuclear Reactor Safety Applications Workshop Proceedings, CFD4NRS-3 Bethesda, Maryland, USA, 14-16 September 2010.

14. Hassan, Y.; Reeves, S.; Stoots, C.; 2016. Experimental CFD Studies of Coolant Flow Mixing Within Scaled Models of the Upper and Lower Plenums of NGNP Gas-Cooled Reactors. Reactor Concepts Research Development and Demonstration. Project No. 12-3759. Report Date: March 30, 2016.

15. Condie, K. G.; McCreery, G. E.; Mcllroy Jr., H. M.; McEligot, D. M.; 2005. Development of an Experiment for Measuring Flow Phenomena Occurring in a Lower Plenum for VHTR CFD Assessment. Idaho National Laboratory. Publication Number: INL/EXT-05-00603.

16. United States Nuclear Regulatory Commission. Westinghouse Technology 3.1 – Reactor Vessel and Internals. Publication Number: ML11223A212. https://www.nrc.gov/docs/ML1122/ML11223A212.pdf (accessed: 03/23/2018)

17. Rumsey, C. L. 2007. Apparent transition behavior of widely-used turbulence models. International Journal of Heat and Fluid Flow, 28, pp. 1460-1471.

18. Allmaras. S. R.,Johnson, F.T. and Spalart, P. R. 2012. Modifications and Clarifications for the Implementation of the Spalart-Allmaras Turbulence Model. Seventh International Conference on Computational Fluid Dynamics (ICCFD7), Big Island, Hawaii, 9-13 July 2012.

19. 2018 Siemens Product Lifecycle Management Software Inc. STAR-CCM+ v 13.02.011–R8 – User guide. (accessed: 03/23/2018)

20. Versteeg, H. K. and Malalasekera, W. 1995. An Introduction to Computational Fluid Dynamics The Finite Volume Method. Longman Scientific & Technical. First edition.

II. CFD ANALYSIS OF TURBULENT FORCED CONVECTION IN THE REACTOR CORE AND FLOW PAST INTERNAL STRUCTURES IN A PWR-TYPE SMALL MODULAR NUCLEAR REACTOR

ABSTRACT

The 800 MWth PWR-type small modular nuclear reactor designed by Westinghouse Nuclear was selected for computational design and thermal-hydraulic analysis. Keeping with established Westinghouse methodology for thermal-hydraulic analysis of PWR fuel assemblies, a 3x3 fuel rod array and spacer grid volumes contained within, were selected as the representative domain. Flow was modeled through a single bottom nozzle. Conditions were extracted downstream of the bottom nozzle and used as inflow conditions for the representative sub-channel. To simulate heat transfer from the fuel rods, two stages of simulations were conducted; stage I simulated the representative volume in its entirety on two levels of mesh refinement, and stage II simulated individual segments of the representative volume along the height of the fuel rod array. While stage I of the simulations required a greater computational effort with the Reynolds Stress Turbulence model, a prediction of the entire sub-channel was developed in one simulation. With stage II of the simulations with the realizable k-ε model, segments of the reactor core could be simulated with less computational effort but required all segments to be simulated before sub-channel analysis could occur. Both stages of simulations concurred with benchmark data, reporting a core outflow temperature in the range of 605 K-607 K, in good agreement with design targets. The outflow profiles from the reactor core were applied as inflow profiles to the upper core and turbulent flow through the upper core was simulated using the realizable k-ε model.

ABBREVIATIONS

PWR	pressurized water reactor
CFD	computational fluid dynamics
SMR	small modular nuclear reactor
WSMR	Westinghouse SMR
RCCA	Rod cluster control assembly
CRDM	Control rod drive mechanism
TPA	Thimble plug assembly
RST	Reynolds Stress Turbulence
MWe	mega-Watt Electric
MWth	mega-Watt Thermal

1. INTRODUCTION

In today's world, it is essential to increase the safety of nuclear energy systems for them to supplant and support conventional energy generation from fossil resources. Conventional PWRs require geographical proximity to cooling sources and site regulations rendering standalone units less desirable for power generation. Small modular nuclear reactors (SMRs) (45 MWe – 330 MWe), have a smaller geographical footprint, are modular in assembly, and are more secure than a conventional PWR; so, they can be used as valuable on-site additions to chemical plants and oil refineries. Studies in this field have proven SMRs to be an economically desirable component of a hybrid energy

system [1]. An SMR can support sensible heat supply for coal-to-chemicals processes, reducing the energy demand from fossil fuels [2]. The motivation of this study is to analyze an SMR, with a focus on the core thermal-hydraulics, using established methodology, previously applied to conventional PWRs [3, 4]. The present design is based on the Westinghouse SMR (WSMR) concept, which integrates a pressurizer and steam generator into the reactor pressure vessel (RPV). The current study focuses on the thermal-hydraulic design and analysis of the reactor core, and upper internals.

CFD has been extensively used to investigate heat generation in the fuel rods, subchannel hydraulics, thermal non-uniformity, flow separation, and mixing patterns. The power rating of a reactor core is primarily dictated by core thermal output. DeCART, a neutronics solver, has been coupled with STAR-CCM+, a commercial CFD code, to predict whole-core transport phenomena at both, subchannel, and core-wide scales [5]. The Consortium for Advanced Simulation of Light Water Reactors (CASL) has provided a verification and validation study for the use of Hydra-TH to predict core single-phase core T-H, GTRF, DNB, and crud induced – power shift, and corrosion [6, 7]. VERA-CS, a core simulator tool developed by CASL, is a whole-core transport code that has demonstrated success on many fuel-related applications when coupled with other 2-D and 1-D formulations [8].

Heat generated in the fuel elements is extracted by forced convection of the coolant in the primary circuit. The turbulent flow from the lower plenum is channeled in to the reactor core through the lower support plate, and the lower core plate. This channeling tends to straighten the flow within the fuel assembly, and the coolant velocity increases due to constricted cross-sectional flow area. To enhance lateral mixing, the

grids that support the fuel rods are fitted with mixing vanes at their top surfaces. Mixing vanes enhance the angular momentum (radial velocity) in the subchannel and reduce lateral thermal non-uniformity. The presence of mixing vanes attenuates the magnitude of vorticity as identified by flow fields captured by particle image velocimetry (PIV) and matched index of refraction (MIR) in a 5x5 rod bundle. [9]. A 5x5 rod bundle with spacer grids was studied for the effect of (i) eleven different angles for split-vane pairs, and (ii) the adverse contribution of peripheral mixing vanes to sub-channel flow distribution in both, experiments and CFD simulations, where a vane angle of 27^0 was identified, beyond which, the increase in pressure loss is not compromised by the gain in heat transfer [10, 11]. Westinghouse also published benchmark data using PIV and MIR, both, upstream, and downstream, of a spacer grid in a 5x5 rod bundle for future use in validating applicable CFD models [12, 13]. PIV measurements at cold test conditions were also used to map the lateral flow field in a typical PWR subchannel to assess the impact of swirl and compared with prior LDV measurements [14].

CFD modeling has allowed for testing alternative designs of mixing vanes, the arrangement on the grid strap, and the impact they have on swirl generation. However, the foundation of this methodology is a major simplification from the physical 17x17 square pitched fuel assembly to a representative 5x5 rod bundle used in experiments, that is further reduced to a 3x3 rod bundle with periodic boundaries to decrease computational costs. The use of flow periodicity at the planes of symmetry for the solid fuel rods in a 3x3 rod bundle, forces cross flow across the periodic interface, capturing which, is a proven limitation of CFD modeling [15, 16]. However, in comparison with experimental data, subsequent CFD modeling of a sub-channel with split-vane pair support grids

showed good agreement with PIV measurements [17]. Convective heat transfer correlations have been developed to predict heat transfer enhancement downstream of support grids for split-vane pair, disc and standard mixing vanes in subchannels [18-20]. CFD has proven useful in predicting the locations of hot spots on fuel rods, as well as the location where DNB occurs, quantified in terms of local hydraulic diameter [21]. Westinghouse methodology for validation and benchmarking of heat transfer in a fully heated rod bundle was conducted by comparing the lateral velocity in a sub-channel, downstream of the spacer grid, and azimuthal variation of heat transfer coefficient around the fuel rod [22]. An important study of relevance beyond validation is the use of CFD in studying lateral forces exerted by turbulent flow on to the fuel rods and quantifying these flow-induced vibrations using large eddy simulations, which are computationally expensive [23].

The work reported in this paper applies existing methodology to predict preliminary T-H behavior in the reactor core. The core outflow passes through varying cross-sections, due to the multi-scale design of upper internals - rod cluster control assemblies (RCCAs), thimble plug assemblies (TPAs), control rod drive mechanisms (CRDMs), upper core plate, upper support plate, transition cone, and the hot leg riser. The subsequent sections describe the physical design of representative volume, the computational domain, and the numerical methodology applied to simulating thermal-hydraulics in the reactor core of this SMR design.

2. MATERIALS AND METHODS

Sub-section 2.1. lists material properties used in the simulations, while sub-section 2.2 explains physical, computational and numerical methodologies used to conduct both sets of simulations.

2.1. MATERIALS

Thermo-physical properties of $UO_{2(s)}$, $He_{(g)}$, $H_2O_{(l)}$ and Zr-$4_{(s)}$ listed in Table 1 are those used in the study established as Westinghouse methodology [3]. The properties have been verified for use in other CFD studies and validated with benchmark hydraulic data for flow through Westinghouse PWR assembly sub-channels [4-5]. Table 1 below lists thermophysical properties of fluids and solids, physics models, and operating conditions used in both simulations.

Table 1. Thermophysical materials properties and operating conditions.

Properties of $UO_{2(s)}$	ρ = 10,400 kg/m^3, C_p = 300 J/kg-K, k = 6 W/m-K
Properties of Zr-$4_{(s)}$	ρ = 6,500 kg/m^3, C_p = 350 J/kg-K., k = 17 W/m-K
Properties of $He_{(g)}$	ρ (ideal gas equation), C_p = 5,181.5 J/kg-K, k = 0.24651W/m-K, μ = 3.0821E-5 Pa-s
Properties of $H_2O_{(l)}$	$(100\ K \leq T \leq 615K)$ $\rho = (34891.3 - 180.573T + 0.321677T^2 - 1.93011 \times 10^{-4}T^3)$ kg/m^3 μ = 9.2062E-5 Pa-s, C_p = 5,122.1 J/kg-K k = 0.59192 W/m-K, (turbulent) Pr = 0.9
Inflow Conditions	4 m/s, 564 K; 2250 psia system pressure

2.2. METHODOLOGY

Sub-sections 2.2.1., 2.2.2., and 2.2.3. respectively describe the physical domain, computational design, and numerical methodology used to execute simulations of flow through the reactor core and upper internals.

2.2.1. Physical Domain. Current design information is based on component information from the AP1000 design by Westinghouse Nuclear. Dimensions of reactor core components and internal structures for the WSMR are scaled down in length from the AP1000, where necessary. Specifications for the WSMR reactor core available in literature, are listed in Table 2 [24].

Table 2. Salient features of the WSMR core.

Thermal Output (MWt)	Electric Output (MWe)	Active Fuel Length (m)	No. of CRDMs	Fuel Assemblies
800	>225	2.4834	37	89

2.2.1.1. Reactor core. The WSMR reactor core consists of 89 17x17 RFA fuel assemblies (<5% enriched U^{235}). The axial length of the active fuel is scaled down to 2.4834 m (8 ft), from about 3.67 m for the AP1000, which requires reducing the number of support grids between the bottom and top nozzles. The estimated design of the fuel assembly and layout of the fuel assemblies within the core baffle is shown in Figure 1. Each bottom nozzle is fed with coolant from four holes in the lower core plate (blue outline).

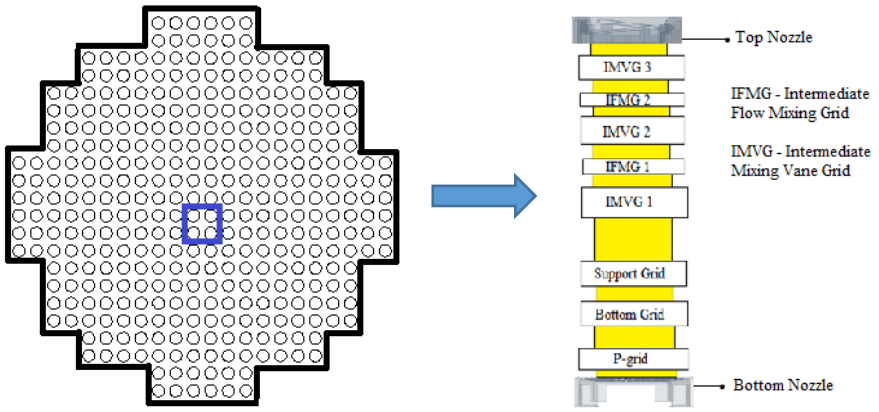

Figure 1. (L-R) A schematic of the core baffle (outline) and holes positioned in the lower core plate; and an elevation view of a representative 17x17 fuel assembly used in the WSMR.

Within the fuel assembly, the support grids hold the fuel elements in place, between the bottom and top nozzles. From bottom to top, are the protective grid (P-grid), a bottom grid, a support grid, and five grids with top mounted split-vane pairs. The latter grids are called intermediate mixing vane grids (IMVGs), and intermediate flow mixing grids (IFMGs). There are 3 IMVGs alternated with 2 IFMGs in the upper core. The IFMGs are half the height of the IMVGs, and serve to re-induce turbulence between the IMVGs, to enhance heat transfer in the upper core where the wall temperatures are near the coolant saturation temperature.

2.2.1.2. Upper internals. The upper internals consist of the upper core plate, RCCAs, TPAs, CRDMs, guide tube assemblies (GTAs), the upper support plate, followed by a transition cone and ‘hot leg riser’. The upper core plate retains pressure on the top nozzles of the fuel assemblies, and the RCCAs/TPAs remain partially inserted in the fuel assemblies, for alignment purposes. In conventional PWR setups, the assemblies that do not receive the RCCAs, are designed to receive TPAs, or burnable poison rod

assemblies (BPRAs). Since this is a preliminary design study, the 37 RCCAs are accompanied by 52 TPAs, to decrease the size of the mesh. The RCCAs/TPAs complete the insertion/retraction aided by the CRDMs, that move through guide tubes, to ensure alignment. The guide tubes and support columns extend between the upper core plate, and the upper support plate. Since the CRDMs are located inside the WSMR, their length is shorter than the core barrel. In a conventional PWR, flow leaving the upper support plate would be considered the 'hot leg' of the reactor. This flow would connect to the external pressurizer unit, and the steam generator(s). In the WSMR design, however, as may be observed in Figure 2, the integral pressurizer and steam generator units receive flow from the hot leg riser. An upper internals plate channels flow leaving the upper support plate, through the transition cone, into the hot leg riser. The hot leg riser transports coolant to the tube side of the annular steam generator.

2.2.2. Computational Methodology. The lateral dimensions of fuel rods and the sub-channel in the representative volume are about two orders of magnitude smaller than the axial span of the representative volume, creating a multi-scale, complex geometry to be discretized in the simulations. Such multi-scale geometries require a wide range of cell sizes to resolve the resulting scales of turbulent flow and heat transfer. To achieve this, certain simplifications were made in the geometric design to reduce the cell count for simulations. A representation is provided in Figure 3.

2.2.2.1. Reactor core models. Flow through the bottom and top nozzles were individually simulated with inflow and outflow conditions from the lower core plate and representative sub-channel volume, respectively. For the representative sub-channel

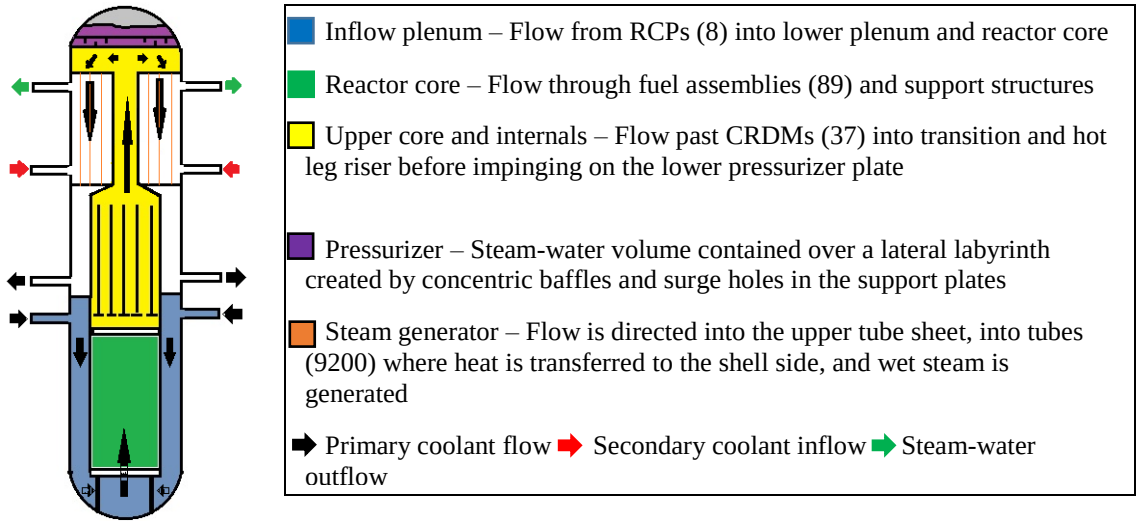

Figure 2. Flow path schematic of the WSMR [24].

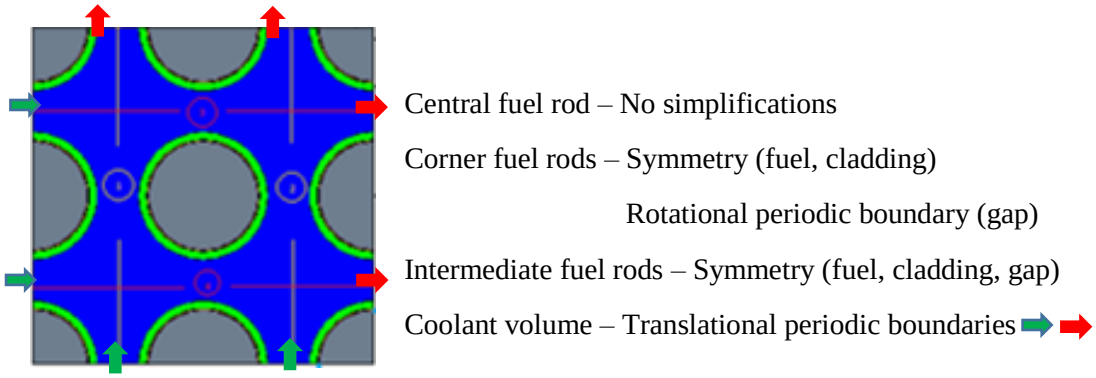

Figure 3. A representation of computational domains in the sub-channel.

volume, two stages of simulations were conducted: the first simulated the entire 3x3 fuel rod array and spacer grids intersecting the sub-channel volume; the second simulated segments of the representative volume along the active length of the fuel, with segment divisions around the spacer grids.

Table 3. CFD model segments, and boundary types.

Model Segments	Bottom Nozzle	
	Full-length of representative volume (3x3 fuel rod array) on two mesh levels	P-Grid Bottom Grid and Support Grid IMVGs and IFMGs
	Top Nozzle	
Fuel	Volumetric heat source; exterior symmetric surfaces (blue)	
Gap	Wall interface; exterior symmetric surfaces	
Cladding	Wall interface; exterior symmetric surfaces (blue)	
Coolant	Wall interface at fuel element surface; translational periodic interfaces across the cross-section	

Table 4. Cell count for simulation domains in both stages of the study.

Stage (i) of reactor core domain simulations.

Model / Zone	Bottom Nozzle (polyhedral)	Full-Length Representative Volume (Mesh 1 - polyhedral)	Full-Length Representative Volume (Mesh 2 - polyhedral)
Coolant	2,106,869	36,948,934	42,104,109
Cladding	-	26,743,358	26,743,358
Gap	-	5,590,800	5,590,800
Fuel	-	1,490,471	1,490,471
		Σ = 70,773,563	Σ = 75,928,738

Stage (ii) of reactor core domain simulations.

Model / Zone	Bottom Nozzle (polyhedral)	P-grid (hexahedral)	Support and Mixing Grids (hexahedral)	Heat Transfer Grids (hexahedral)
Coolant	2,106,869	5,178,825	16,519,850	12,962,364
Cladding	-	2,731,971	6,123,377	6,330,796
Gap	-	1,768,083	2,218,923	8,171,808
Fuel	-	1,426,896	240,128	4,154,640

The second stage thus simulated the following domains: the P-grid; the bottom and support grids; and the intermediate flow mixer and mixing vane grids (IFMG, IMVG). The simulation domains and types of boundary conditions used are summarized in Table 3. A primary motivation for the second stage of simulation was to check if local mesh refinement yielded results similar to those from a sub-channel level simulation. Table 4 lists the cell count from all simulation domains for comparison.

For stage I of the simulations, the Reynolds Stress Turbulence (RST) model was used to simulate turbulent flow since there is little work published in simulating such a domain. The RST model is known to provide, at a higher computational cost, a thorough contribution of all stress terms in its numerical formulation which is expected to yield a better initial estimate for a preliminary study. For stage II of the simulations, however, experimental hydraulic data from the inflow volume (P-grid, bottom grid) have previously been compared over a range of inflow velocities with CFD simulations, where the realizable k-ε model was found to predict a pressure drop closest to experimental values [26]. The study considered only a quarter of the bottom nozzle, P-grid, and bottom grid, due to the geometric complexity. In the current design, the bottom nozzle is modeled in its entirety. The realizable k-ε model is used to quantify turbulent parameters in the bottom nozzle simulation, so that recirculation parameters may be well resolved based on previous studies on pressure loss through the perforated plate of a bottom nozzle [27]. The bottom nozzle model simulates flow through a single nozzle, detailed with a perforated plate at the top of the bottom nozzle, which consists of several patterns of holes, and the outflow from the nozzle is extracted 3 mm downstream of the perforated plate, and input to the P-grid model. Piece-wise modeling allows detailed flow resolution

for pre-determined portions of the reactor core at a lower computational cost. Each simulation was run at the system pressure of 2250 psia until outflow kinetic energy and temperature reached stable values. The realizable k-ε model is used to characterize turbulent flow in the coolant domain for all the reactor core simulations. Averaged outflow conditions from the mixing grids model were used as inlet boundary conditions to simulating flow through the upper core. Figure 4 shows 3D CAD representations of bottom and top nozzles.

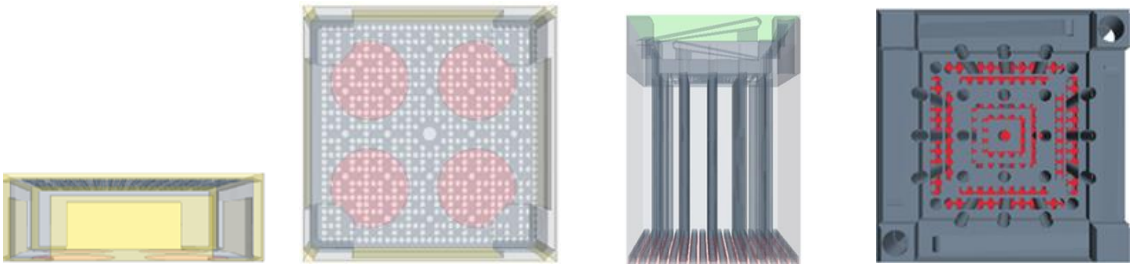

Elevation View Top View Elevation View Top View

Figure 4. (L-R) 3D CAD model used to simulate flow through (L) a single bottom nozzle (elevation and top views) and (R) a single top nozzle (elevation and top views).

2.2.2.2. Upper core model. The upper internals model uses the outflow from the top nozzle model as the input and is applied to the inflow for all 89 fuel assemblies. The locations of the 37 internal CRDMs/RCCAs are shown in Figure 5. The unblocked flow area gradually increases with height of the reactor beyond the top nozzle, up until the transition cone. The upper end of the hot leg riser is considered the outlet for this model. The upper core plate, upper support plate, and upper internals plate for the SMR are all configured with an unblocked flow area of 2400 in^2. The holes in the upper core plate are fitted in between the RCCA inserts, and the support columns.

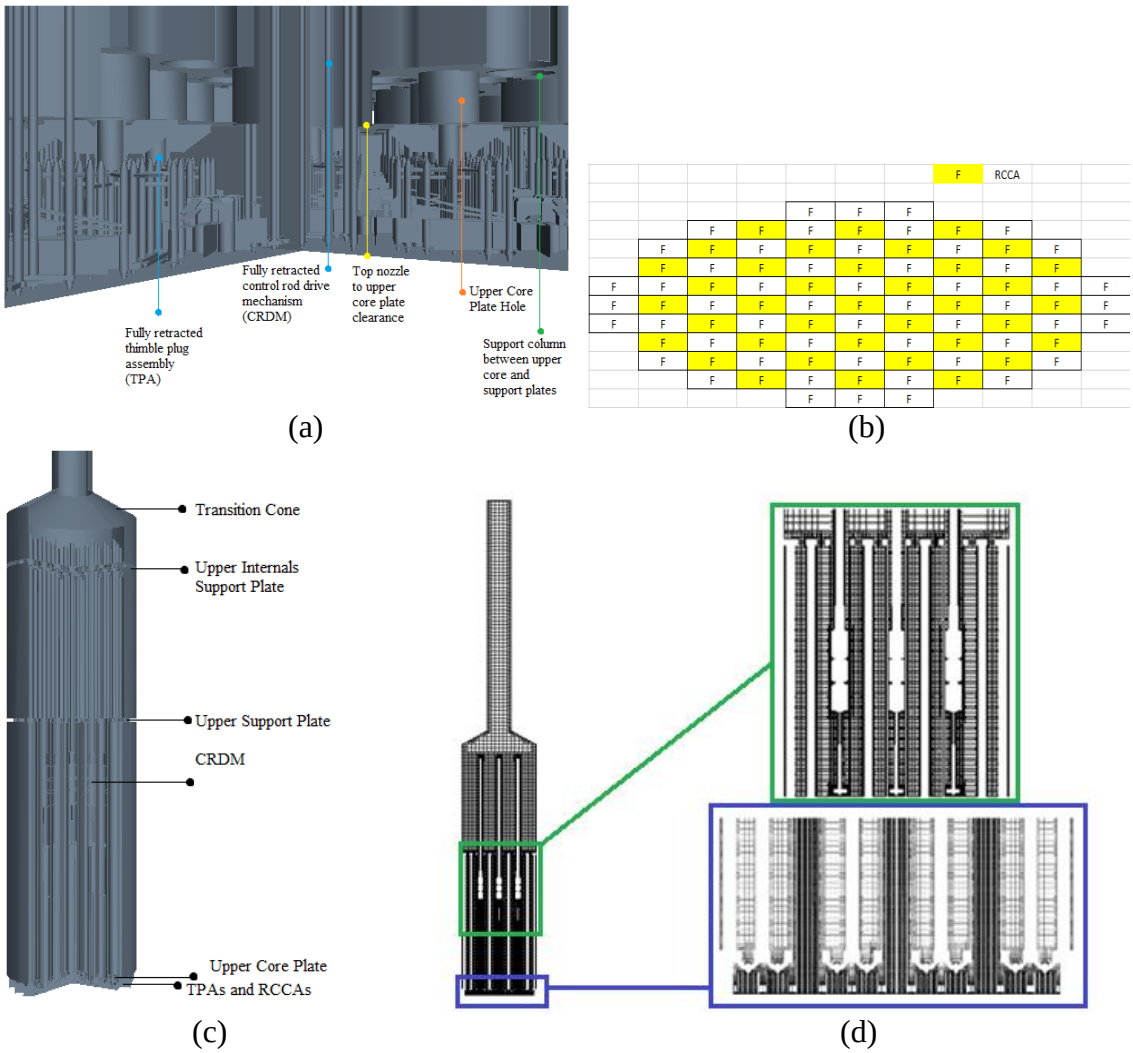

Figure 5. (a) Geometric detail of the upper core simulation domain (b) layout of fuel assemblies within the core baffle and location of RCCAs (c) flow path through the upper core and (d) mesh detail on a representative axial cross-section plane through the upper core simulation domain.

The holes in the upper support plate are fitted in between the support columns and guide tubes. The upper internals plate is designed with circular holes evenly distributed on the plate cross-section area. All the solid structures are subtracted from the upper core volume, and only the flow volume is modeled. The CFD simulation was conducted on a

mesh consisting of 101,146,361 hexahedral cells. Figure 5 shows the geometry and mesh representation of the upper core simulation.

3. RESULTS

Simulations of thermal-hydraulics through the bottom nozzle, top nozzle, and stage II of the reactor core were conducted on a Lenovo NeXtScale cluster running CentOS 6.7 on six Lenovo nx360m5 compute nodes with a total of 120 CPUs, 48 TB HDD memory, and 364 GB RAM. Stage I of the reactor core simulation was conducted at the Oak Ridge Leadership Computing Facility, Oak Ridge National Laboratory, USA, using 20 compute nodes (320 CPUs) on Rhea.

3.1. BOTTOM NOZZLE

The volume between the support legs of the bottom nozzle provide an expansion for flow emanating from the holes of the lower core plate. The top plate of the bottom nozzle and the P-grid are separated by a 5 mm clearance. Accordingly, the outflow profile is extracted 3 mm above the top plate of the bottom nozzle.

Three simulations of flow through the bottom nozzle were conducted on 1.72 M, 2.1 M, and 13 M cells respectively. The area-averaged velocities at the outlets of the models were respectively calculated to be 2.74 m/s, 2.98 m/s, and 2.61 m/s. Figure 6 compares the linear lateral variation in magnitude of velocity in the three calculations, at a location 3 mm above the top plate of the bottom nozzle.

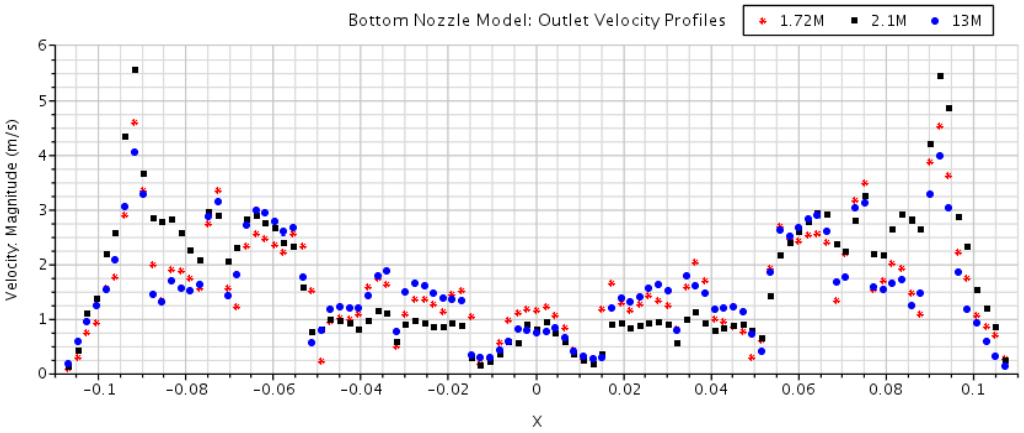

Figure 6. Outflow profiles from the bottom nozzle model.

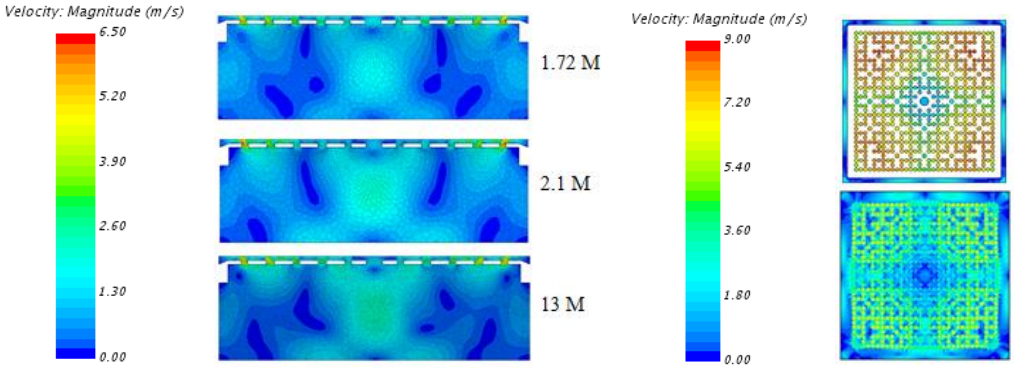

Figure 7. Velocity profiles at (L) central axial cross-section planes and (R) (top) geometric upper surface of the bottom nozzle, (bottom) domain outlet 3 mm above. perforated plate.

Figure 7 shows the velocity variation across a central, axial plane for the three simulations. Also, the lateral cross-section at a 3 mm elevation above the top plate is shown. The profile at the true upper surface of the plate is provided for comparison. It msy be inferred that the coarser meshes are able to predict flow separation along the height of the domain but not resolve zero velocity zones near the sharp edges and in the

near-wall cells. The 13M mesh is able to clearly resolve these recirculation zones near the sharp edges, suggesting a more accurate contribution to flow through the holes of the Outflow velocity values from the domain outlet were exported and used as an inlet boundary condition for stages I and II of the reactor core simulations.

3.2. SIMULATION OF REPRESENTATIVE 3x3 SUB-CHANNEL DOMAINS

3.2.1. Stage I: Full-Length Representative Volume. Two levels of mesh refinement were used in stage I of the simulations. Figure 8 shows the locations of four sampling probes used to report fuel rod centerline temperatures in the sub-channel volume and the profiles reported by simulations on both meshes. Figure 9 and Figure 10 show the locations of four sampling probes used to report sub-channel coolant temperatures and turbulent kinetic energy along the length of the sub-channel, respectively.

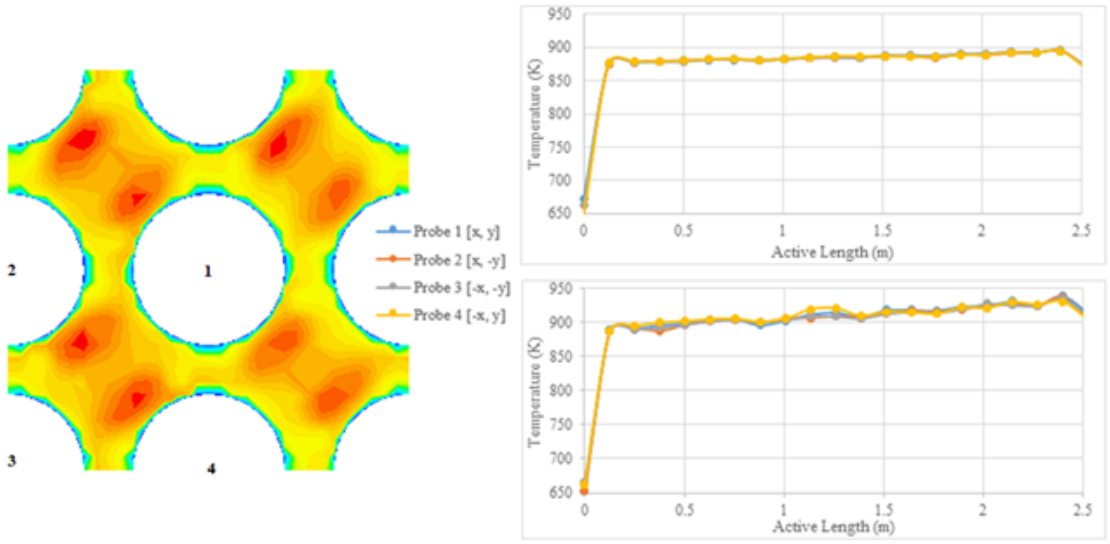

Figure 8. (L-R) Fuel centerline temperature profiles sampled at four locations (L) along the active length on a coolant mesh (R) with (top) 13.3 M cells and (bottom) 42 M cells.

From Figure 8, it is inferred that both simulations report qualitatively similar centerline temperatures for the fuel rods in the sub-channel. Between the two simulations, only the mesh discretizing the coolant domain was refined. This suggests that near-wall mesh refinement in the coolant domain affects the dissipation of heat in the sub-channel. Figure 9 below compares wall temperatures reported by both simulations for the central fuel rod, and the temperature profiles in the sub-channel along the active length of the fuel rods.

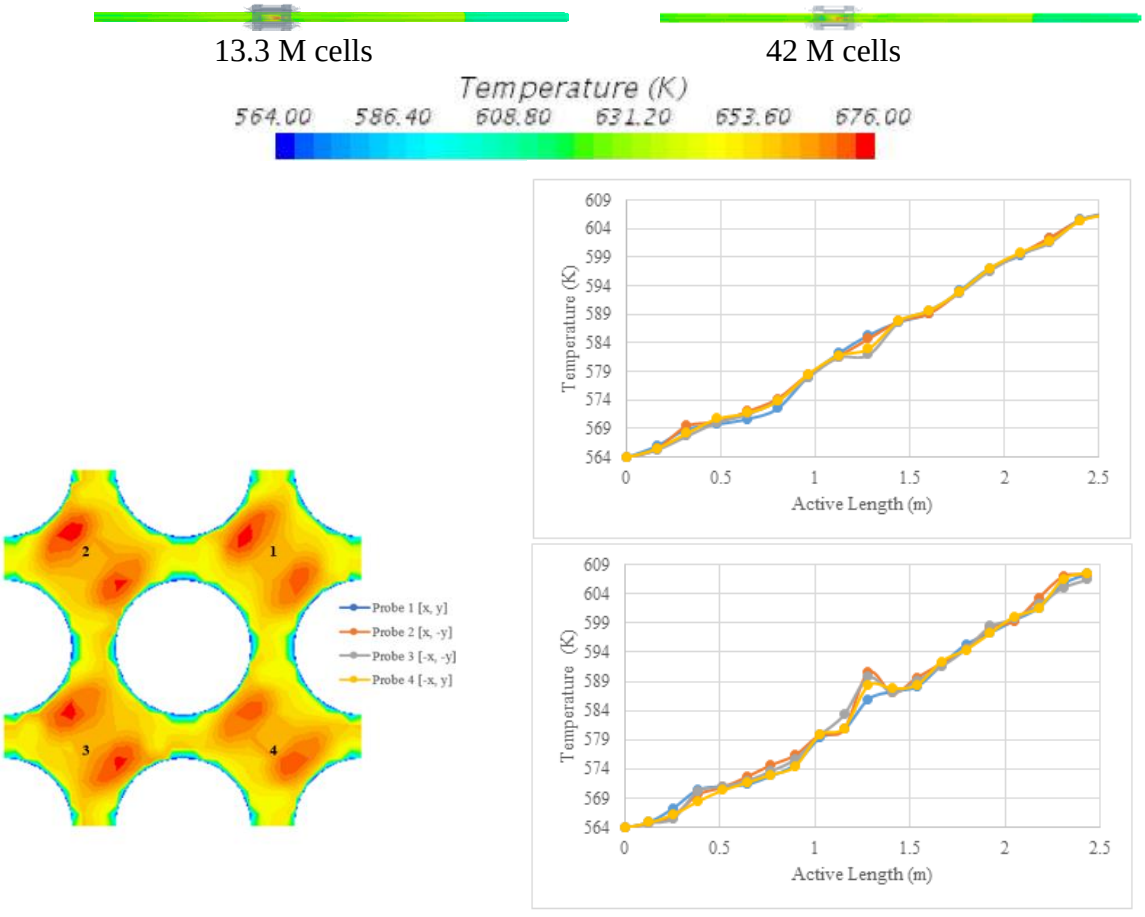

Figure 9. (L-R) Sub-channel coolant temperature profiles sampled at four locations (L) along the active length on a coolant mesh (R) with (top) 13.3 M cells and (bottom) 42 M cells. Central fuel rod temperatures from both simulations provided for reference.

Figure 10 and Figure 11 respectively compare the sub-channel profiles for turbulent kinetic energy of the coolant, and axial 2D temperature profiles in the sub-channel. It may be observed that mesh refinement in the coolant domain is able to capture sharper perturbations in turbulent kinetic energy at locations identical to those from the coarser mesh, which suggests that the local velocity profiles show significant fluctuations as well. This abrupt variation in velocity can be inferred to affect local lateral thermal profiles and downstream heat removal. This may be noted by coolant temperature profiles in Figure 12.

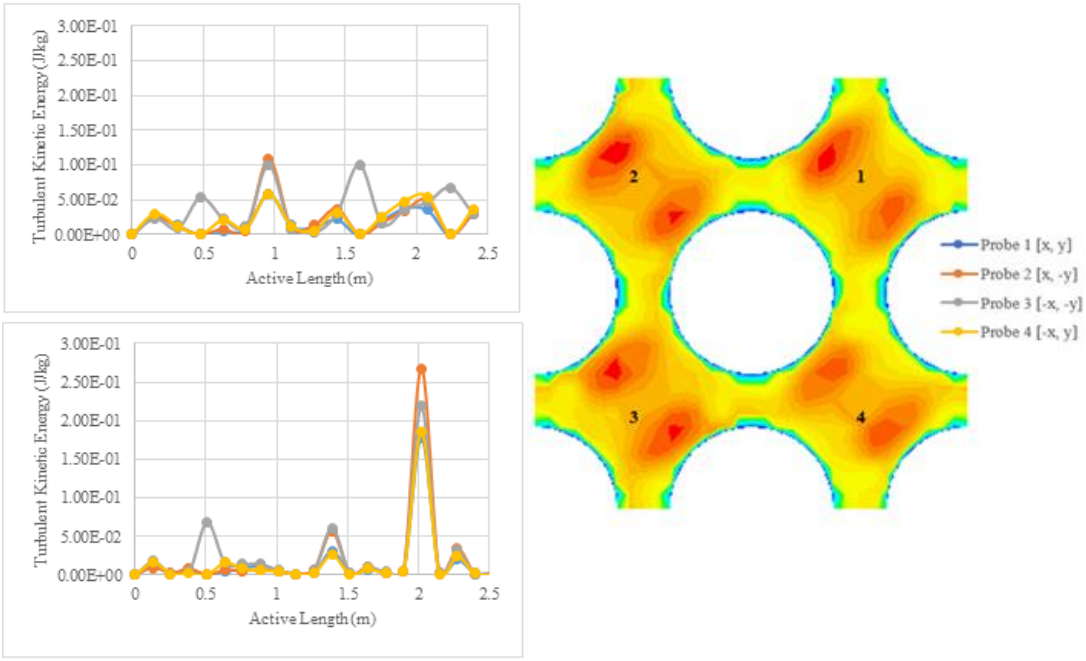

Figure 10. Turbulent kinetic energy profiles along the active length of the sub-channel from the simulation of a coolant mesh with 42 M cells.

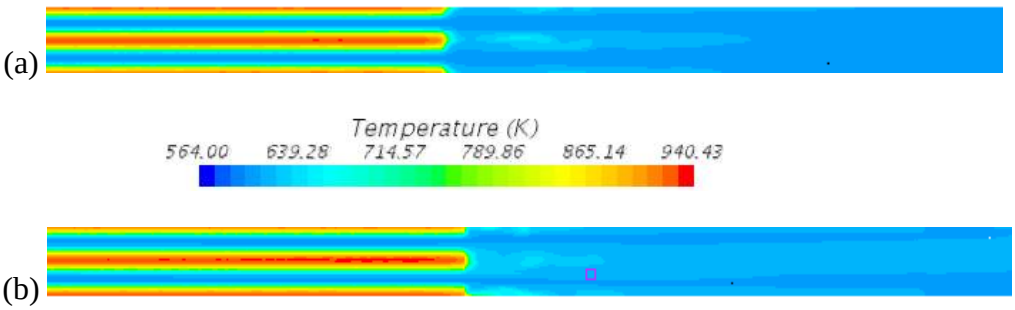

Figure 11. Temperature profiles of core outflow across a central axial cross-section plane reported by simulations on coolant mesh with (a) 37M cells and (b) 42M cells.

3.2.2. Stage II: Piece-wise Simulation of Representative 3x3 Sub-Channel.

3.2.2.1. P-grid. Structurally, the P-grid serves to induce preliminary turbulence to straightened flow entering from the bottom nozzle as channeled flow to the fuel rods, for heat removal. The flow exiting the support grids is averaged at about 573 K, and 3.8 m/s. Figure 12 shows the velocity and temperature profiles downstream of the P-grid.

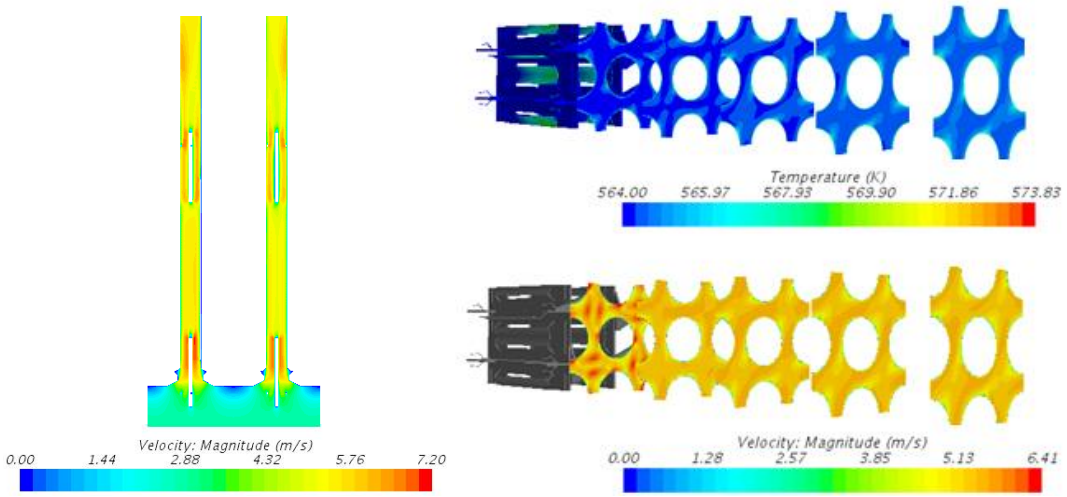

Figure 12. Axial variation in velocity (L) and lateral variation in temperature and velocity (R) downstream of the P-grid.

3.2.2.2. Bottom and support grid. Figure 13 shows the impact of mixing vanes on downstream flow. Flow through the bottom grid, devoid of mixing vanes, emerges with a cold spot in each sub-channel, with higher coolant temperatures in the fuel rod periphery. In contrast, flow exiting the mixing grid shows the breakup of lateral vortices, with downstream flow exhibiting relative uniformity in temperature.

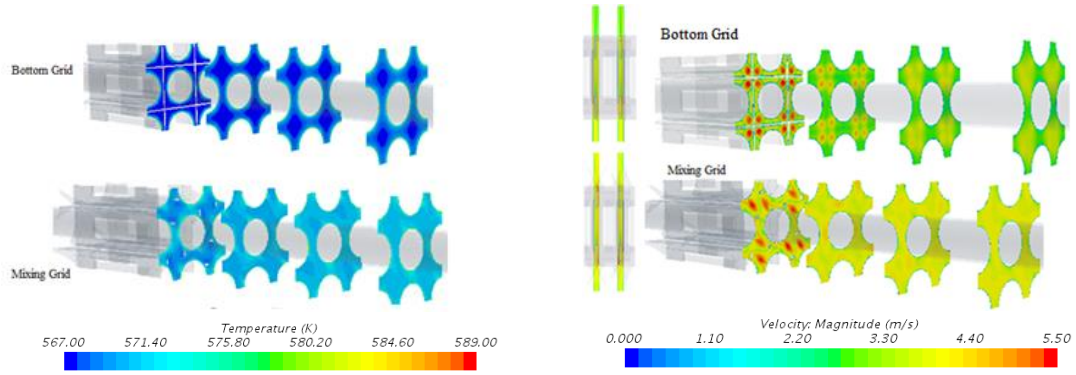

Figure 13. Lateral variations in downstream profiles of (L) temperature and (R) velocity.

3.2.2.3. Intermediate mixing grids and intermediate flow mixers. Figure 14 provides the temperature variation on the fuel rods in the Heat Transfer Grids model. The simulation reported area-averaged temperature and velocity values for core outflow at 605 - 609 K and 4.13 m/s, respectively. Figure 9 also compares temperature data around the fifth spacer grid with mixing vanes (Yan, J. et al), with the current results (WSMR) [4]. The established averaged core outflow temperature is 603 K – 605 K. Both values are below the saturation temperature of 617 K, at the system pressure.

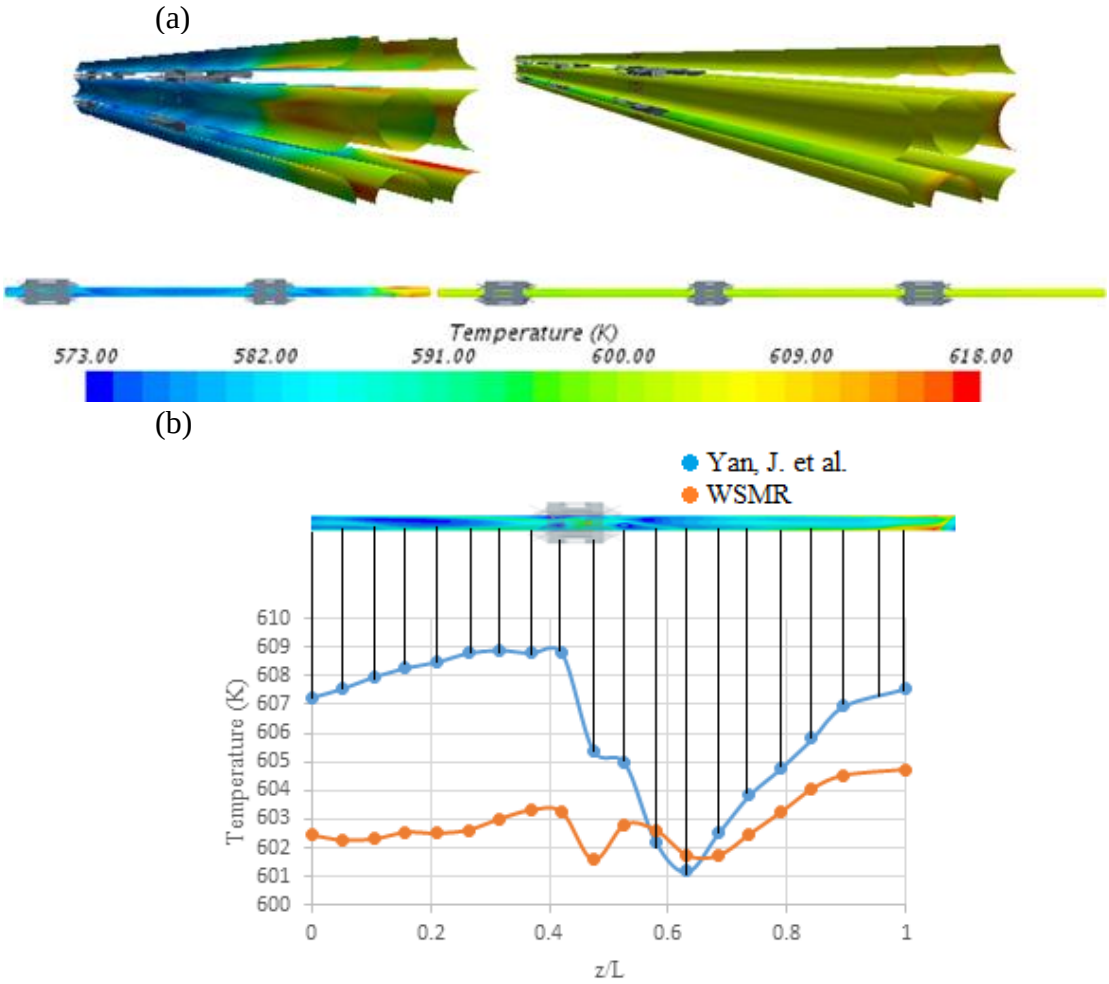

Figure 14. Temperature profiles in (a) the sub-channel coolant walls and (b) central fuel rod [4].

It may be noted that turbulence induced by split-vane pairs on the grids are responsible for promoting heat transfer. Induced swirl prolongs flow detachment and retains a vortex core in the rod gap widths. The highest velocity in the rod gap widths is observed to be on the cross-sectional plane immediately following the trailing edge of mixing vanes and dissipates with downstream flow. Figure 15 shows the trailing edge of each grid is used as a reference elevation on the fuel rod, and the planes are spaced at regular intervals after each grid.

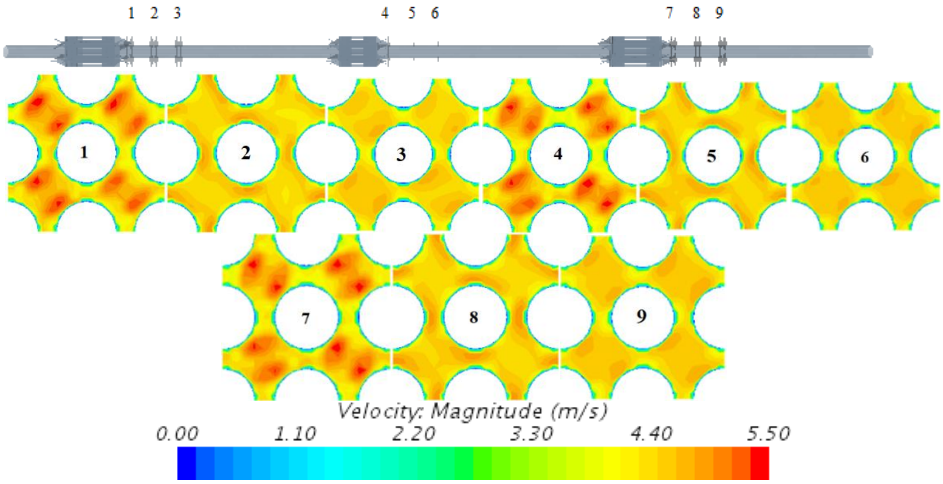

Figure 15. Swirl formation at the vane end of the grids, and lateral dissipation of downstream vortices.

3.3. UPPER CORE

Core outflow was input to simulating flow through the upper core and internals, which included the upper end of the fuel rods, and the coolant volume below the perforated plate of the top nozzle. Flow enters through the perforated plate in the top nozzle, faces an enhancement in available cross-sectional area, and then a constriction again, while flowing past the TPAs and RCCAs. After flowing through the hold-down devices for respective assemblies, the flow accelerates due to constriction in area, and generates high velocity jets as observed in Figure 16. The outflow profile from the top nozzle model was applied as an averaged condition to all 89 top nozzles in the reactor core. While the 37 RCCAs are modeled in complete retraction, the 52 TPAs pose a significant blockage to the top nozzle outflow, creating an evident rise in the guide tube velocity magnitude. In the TPA guide tubes, the bulk velocity magnitude is observed to be around 8 m/s, and the instantaneous velocities due to constrictions are at, or above 20 m/s.

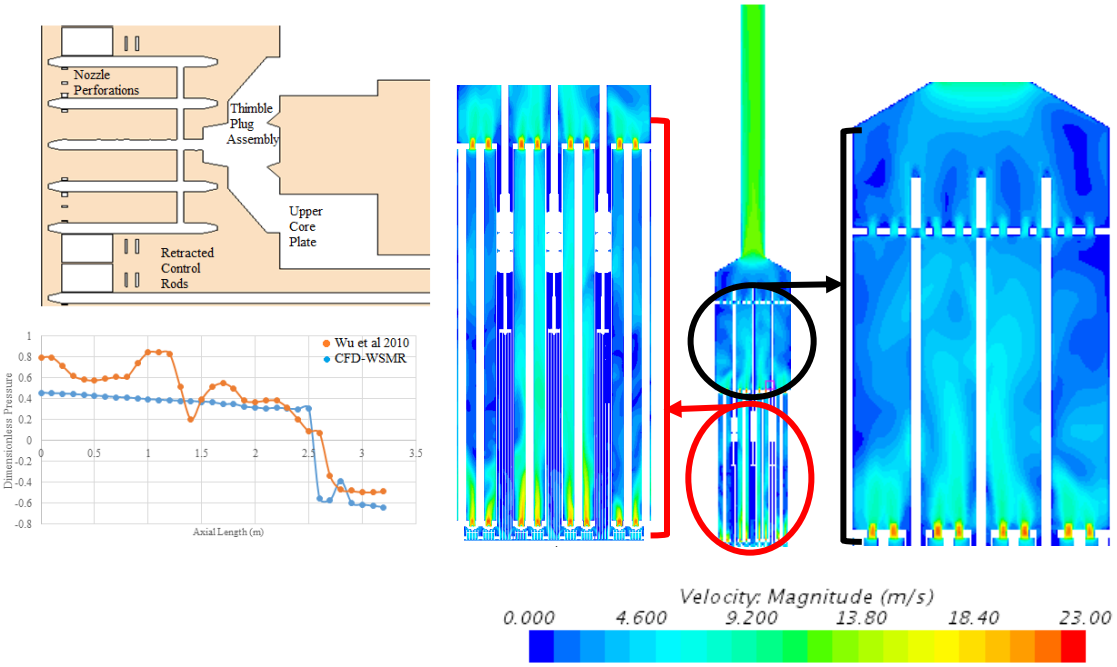

Figure 16. (L-R) Pressure and velocity variations in the upper core [28].

The RCCA guide tubes show relatively uniform convective flow throughout the upper core. Unlike previous CFD studies on the upper core, the current model makes absolutely no geometric simplifications in the upper core. The profile observed in Figure 16 is qualitatively similar from that previously studied for the top nozzle region [28,29]. Figure 16 compares the static pressure in the current study (WSMR) with a previous study of pressure variation in the upper core (Wu et al, 2010).

The transition cone and hot leg riser seamlessly channel flow above the upper internals plate towards the pressurizer. The velocity magnitude at the top of the hot leg riser is averaged at 11.924 m/s, with an axial velocity component of 11.922 m/s. The variation in velocity profiles with increasing elevation in the upper core model is shown in Figure 17.

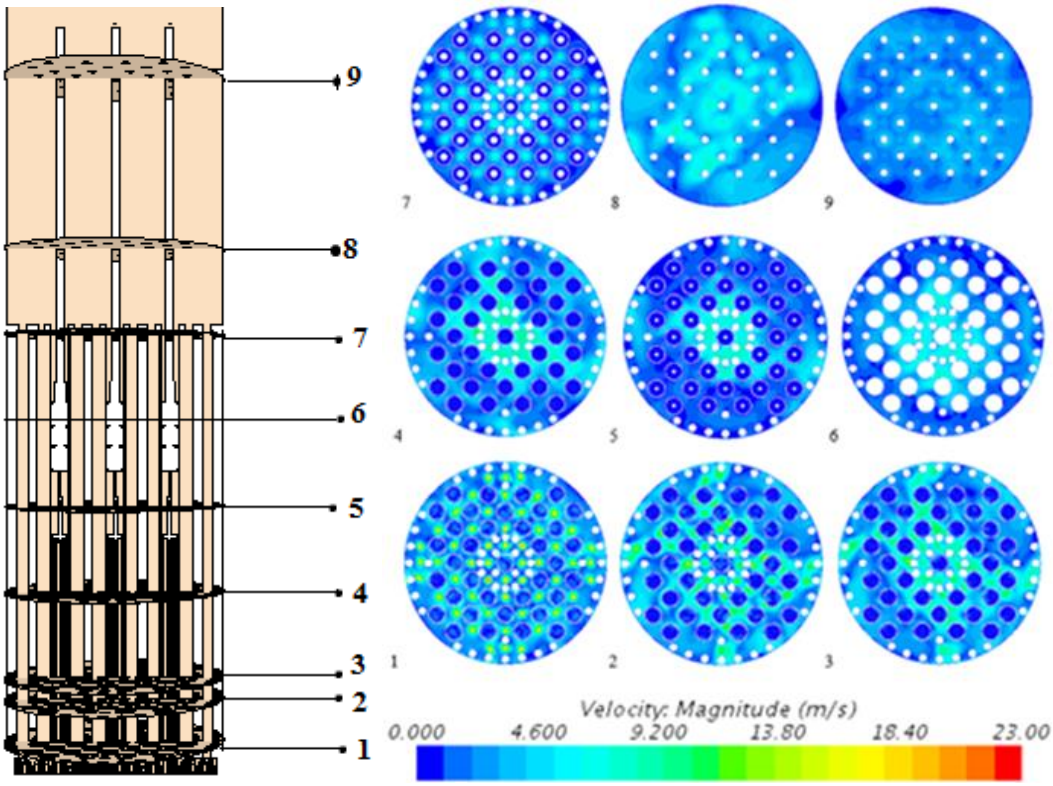

Figure 17. Flow profiles at cross-section elevations in the upper core.

4. CONCLUSIONS

Computational design of the reactor core and upper internals in a PWR-type small modular nuclear reactor was conducted, on which, thermal-hydraulic simulations and analyses were carried out using commercial CFD package, STAR-CCM+ v. 11/12. The physical design of the reactor core was discussed, based on which, a computational methodology was established keeping in conformity with established methodology used by Westinghouse Nuclear. Within the reactor core, a single 17x17 fuel assembly was chosen as the design space. Flow through a single bottom nozzle was simulated to obtain flow conditions prior to contact with the fuel rods. Then, a representative sub-channel volume was selected with a 3x3 fuel rod array and associated spacer grid volumes

contained within. This was performed to reduce the computational requirements to analyze the multi-scale geometry in a 3D computational mesh, with solid surfaces in the sub-channel volume simulated as symmetric surfaces for further simplification. The fluid surfaces were set as periodic interfaces in linear translation, while the central fuel rod in the sub-channel array was simulated in its entirety. Two stages of simulation were conducted to evaluate the relative accuracy of simulating an entire sub-channel volume as opposed to a greater mesh resolution on smaller segments of the sub-channel divided axially along the active length of fuel rods, with the outflow conditions from the upstream segment then set as inflow conditions to subsequent downstream segments. Stage I of simulations for the entire sub-channel volume was conducted using the RST model to resolve turbulent flow phenomena due to the first-of-a-kind approach used in this study, and the reliability of the RST model to provide a better representation of turbulent flow through a relatively fine mesh, where model validation had not yet been conducted for other RANS models. Stage II of simulations was conducted with the study in conformity with established Westinghouse methodology using the realizable k-ε model which had been proven to better predict pressure drop in the inlet region of a Westinghouse PWR fuel assembly.

Temperature, velocity, and turbulent kinetic energy variations in the sub-channel were compared for both stages of the simulation. It was observed that piece-wise simulation of the reactor core was able to report qualitatively similar profiles, as well as quantitatively similar values as the sub-channel level simulation at a reasonable computational cost. Also, the locations of perturbations in turbulent kinetic energy identified during stage I of the simulations indicated sharp local fluctuations in local

velocity downstream of mixing vanes as verified by mesh refinement in the near-wall region of the coolant domains. Additionally, this was observed to affect heat retention with the fuel rods noted by higher centerline temperatures in the simulation with mesh refinement for the coolant domain. Figure 10 and Figure 15 indicated that the temperature profiles reported in the sub-channel during both stages of simulations were in good agreement, and the core outflow temperature could be averaged between 605 K – 607 K, which surpasses the design target of 615^0F (597 K), and is below the saturation temperature of ~617 K.

Outflow profiles from the reactor core simulations were imported as inflow profiles to simulate flow through the upper core and past internals. This domain included top nozzles for all 89 fuel assemblies, the upper core plate, 37 CRDMs, and 52 TPAs used as place-holders to retain geometric alignment of all fuel assemblies with the upper core plate. Flow past the RCCAs and through the upper support plate were simulated, and profiles for outflow through the transition cone and hot leg riser were obtained. This simulation of turbulent flow was conducted using the realizable k-ε model, and turbulent flow was resolved through the new component volumes – the transition cone, and hot leg riser.

ACKNOWLEDGEMENTS

The authors would like to thank Westinghouse Electric Company LLC for guidance in the CFD study; the Missouri Technology Corporation, the Small Modular Reactor Research and Education Consortium (SMRREC) and Missouri University of

Science & Technology for financial support that made this work possible. Lastly, the authors are grateful to the computational resources made available at Oak Ridge National Laboratory's Oak Ridge Leadership Computing Facility.

REFERENCES

1. Buchheit, K. L., Smith, J. D., Guntupalli, U., Chen, C., 2016. Techno-Economic Analysis of a Sustainable Coal, Wind, and Nuclear Hybrid Energy System. Energy Fuels, *30* (12), pp 10721-10729.

2. Gandrik, A. M., and Wood, R. A., 2010. HTGR-Integrated Coal to Liquids Production Analysis. Coal-Derived Products, 2010 International Pittsburgh Coal Conference, Istanbul, Turkey.

3. Karoutas, Z., Yan, J., Conner, M., Mandour, A., 2011. Advanced Thermal Hydraulic Method Using 3x3 Pin Modeling. The 14th International Topical Meeting on Nuclear Reactor Thermal Hydraulics, NURETH-14, Toronto, Ontario, Canada, September 25-30, 2011, NURETH14-338.

4. Yan, J., Kochunas, B., Hursin, M., Downar, T., Karoutas, Z., Baglietto, E., 2011. Coupled Computational Fluid Dynamics and MOC Neutronic Simulations of Westinghouse PWR Fuel Assemblies with Grid Spacers. The 14th International Topical Meeting on Nuclear Reactor Thermal Hydraulics, NURETH-14, Toronto, Ontario, Canada, September 25-30, 2011, NURETH14-254.

5. Kochunas, B., Stimpson, S., Collins, B., Downar, T., Brewster, R., Baglietto, E., Yan, J. 2012. Coupled Full Core Neutron Transport/CFD Simulations of Pressurized Water Reactors. PHYSOR 2012 – Advances in Reactor Physics – Linking Research, Industry, and Education. Knoxville, Tennessee, USA, April 15-20.

6. Baglietto, E., Christon, M. A., Bakosi, J., Magolan, B. L., Manera, A., Petrov, V., Smith, T. M., 2014. Single Phase Validation of Hydra-TH for Fuel Applications. Consortium for Advanced Simulation of LWRs. August 30, 2014. CASL-U-2014-0154-000.

7. Magolan, B. L. 2015. Implementation of a Non-Linear Eddy Viscosity Turbulence Model into Hydra-TH for Fuel Related Applications. Master of Science thesis. Massachussets Institute of Technology.

8. Franceschini, F. 2015. AP1000® PWR Startup Core Modeling and Simulation with VERA-CS. Consortium for Advanced Simulation of LWRs. March 26, 2015. CASL-U-2015-0132-000.

9. Dominguez-Ontiveros, E. E. and Hassan, Y. A., 2009.Non-Intrusive Experimental Investigation of Flow Behavior Inside a 5x5 Rod Bundle with Spacer Grids using PIV and MIR. Nuclear Engineering and Design 239, pp. 888-898.

10. Navarro, M. A., and Santos, A. A. C., 2009. Numerical Flow Simulation of Spacer Grids with Mixing Vanes in a 5x5 PWR Rod Bundle. Proceedings of the 17th International Conference on Nuclear Engineering ICONE17, July 12-16, 2009, Brussels, Belgium.

11. Navarro, M. A. and Santos, A. A. C., 2009. Numerical Evaluation of Flow through a 5x5 PWR Rod Bundle: Effect of the Vane Arrangement in a Spacer Grid. 2009 International Nuclear Atlantic Conference – INAC 2009, Rio de Janeiro, Brazil, September 27 to October 2, 2009. Associacao Brasileira de Energia Nuclear – ABEN.

12. Dominguez-Ontiveros, E. E., Hassan, Y. A., Conner, M. E., Karoutas, Z., 2012. Experimental Benchmark Data for PWR Rod Bundle with Spacer-Grids. Nuclear Engineering and Design 253, pp. 396-405.

13. Conner, M. E., Hassan, Y. A., Dominguez-Ontiveros, E. E., 2013. Hydraulic Benchmark Data for PWR Mixing Vane Grid. Nuclear Engineering and Design, 264, pp. 97-102.

14. Baglietto, E. and Ninokata, H. Selection of an Appropriate Turbulence Modeling in a CFD Code for an Ultra-Long Life Core for the “IRIS” Reactor. GENES4/ANP2003, Sep. 15-19, 2003, Kyoto, Japan. Paper 1153.

15. McClusky, H. L., Holloway, M. V., Beasley, D. E., Conner, M. E., 2002. Development of Swirling Flow in a Rod Bundle Subchannel. Journal of Fluids Engineering. 124, pp. 747-755.

16. Liu, B., Dzodzo, M. B., Paramonov, D. V., Smith, L.D. III, Conner, M. E., Young, M. Y., 2004. Application of CFD in the Design Process for PWR Spacer Grid Mixing Vanes. 2004 International Meeting on LWR Fuel Performance; Technical Track 1 – Advances in Nuclear Fuel Design and Fabrication.

17. McClusky, H.L., Holloway, M. V., Conover, T. A., Beasley, D. E., Conner, M. E., Smith, L. D. III, 2003. Mapping of the Lateral Flow Field in Typical Subchannels of a Support Grid with Vanes. Journal of Fluids Engineering. 125, pp. 987-996.

18. Holloway, M. V., Conover, T. A., McClusky, H. L., Beasley, D. E., Conner, M. E., 2005. The Effect of Support Grid Design on Azimuthal Variation in Heat Transfer Coefficient for Rod Bundles. Transactions of the ASME. 127, pp. 598-605.

19. Holloway, M. V., Beasley, D. E., Conner, M. E., 2006. Investigation of Swirling Flow in Rod Bundle Subchannels Using Computational Fluid Dynamics. Proceedings of ICONE14, International Conference on Nuclear Engineering, July 17-20, 2006, Miami, Florida, USA.

20. Holloway, M. V., Beasley, D. E., Conner, M. E., 2007. Single-Phase Convective Heat Transfer in Rod Bundles. Nuclear Engineering and Design. 238, pp. 848-858.

21. Ikeda, K., Makino, Y., Hoshi, M., 2005. Single-Phase CFD Applicability for Estimating Fluid Hot-Spot Locations in a 5x5 Fuel Rod Bundle. Nuclear Engineering and Design. 236, pp.1149-1154.

22. Conner, M. E., Baglietto, E., Elmahdi, A. M., 2010. CFD Methodology and Validation of Single-Phase Flow in PWR Fuel Assemblies. Nuclear Engineering and Design 240, pp. 2088-2095.

23. Elmahdi, A. M., Lu, R., Conner, M. E., Karoutas, Z., Baglietto, E., 2011. Flow Induced Vibration Forces on a Fuel Rod by LES CFD Analysis. The 14th International Topical Meeting on Nuclear Reactor Thermal Hydraulics (NURETH-14), Hilton Toronto Hotel, Toronto, Ontario, Canada, September 25-29, 2011. NURETH14-365.

24. Westinghouse Electric Company, LLC. http://www.westinghousenuclear.com/New-Plants/Small-Modular-Reactor. (accessed 08/14/2017)

25. United States Nuclear Regulatory Commission. Westinghouse Technology Systems Manual. https://www.nrc.gov/docs/ML1122/ML11223A212.pdf. (accessed 12/04/2012)

26. Yan, J., Yuan, K., Tatli, E., Huegel, D., Karoutas, Z., 2012. CFD Prediction of Pressure Drop for the Inlet Region of a PWR Fuel Assembly. Computational Fluid Dynamics (CFD) for Nuclear Reactor Safety Applications - Workshop Proceedings, CFD4NRS-3 - Experimental Validation and Application of CFD and CMFD Codes to Nuclear Reactor Safety Issues, January 2012 (p. 1231). Nuclear Energy Agency of the OECD (NEA).

27. Barros Filho, J. A., Navarro, M. A., dos Santos, A., Jordao, E. 2011. Experimental and CFD Simulations of Pressure Loss through Perforated Plates. Journal of Energy and Power Engineering 5, pp. 112-121.

28. Wu, C-Y., Kao, T-T., Chieng, C-C., Yuan, K., Dzodzo, M. B., Conner. M. E., Beltz, S. A., Ray, S., 2010. CFD Analysis of PWR Core Top Region – Top Fuel Assembly and Top Nozzle regions. Proceedings of the 18th International Conference on Nuclear Engineering ICONE18, May 17-21, 2010, Xi'an, China.

29. Xu, Y., Conner, M., Yuan, K., Dzodzo, M. B., Karoutas, Z., Beltz, S. A., Ray, S., Bissett, T. A., Chieng, C-C., Kao, M-T., Wu, C-Y., 2012. Study of Impact of the AP1000® Reactor Vessel Upper Internals Design on Fuel Performance. Nuclear Engineering and Design 252, pp. 128-134.

III. CFD DESIGN AND ANALYSIS OF TURBULENT HEAT TRANSFER THROUGH THE INTEGRAL PRESSURIZER UNITAND ONCE-THROUGH STEAM GENERATOR IN A PWR-TYPE SMALL MODULAR NUCLEAR REACTOR

ABSTRACT

Turbulent flow through the integral pressurizer unit of a PWR-type small modular nuclear reactor was simulated using commercial CFD package – STAR-CCM+ v. 12. Four turbulence models based on the Reynolds Averaged Navier Stokes (RANS) equations were used to capture hydrodynamics in the plenum intermediate to the integral pressurizer and integral steam generator unit. The selected unsteady RANS models were the realizable k-ε model, the SST k-ω model, the Reynolds stress model (RSM), and the Spalart-Allmaras model. A sufficiently fine mesh was generated with near-wall y+ values nearly equal to 1 or less, upon which turbulent flow was simulated using individual turbulence models. Of the four, the RSM was observed to predict near-zero velocity zones in the interior flow, as well as high velocity zones only in the cell layers adjacent to the lower pressurizer plate. The other turbulence models were observed to over-predict the presence of high velocity zones, while displaying diffused profiles for the interior flow. The greater reliability of the RSM prediction was attributed to the contribution from additional stress terms in the numerical formulation. RSM was further used to model turbulent flow into the upper tube sheet of the integral once-through steam generator. Hydrodynamic profiles for the tube-side were reported and heat transfer to the shell-side was quantified in terms of steam quality at the shell outlet. The steam production was reported to be 58% by volume, with a design target of 60%. Thus, the RSM predictions were taken with statistical confidence.

1. INTRODUCTION

Thermodynamic stability for PWR systems is primarily controlled by a pressurizer unit. In conventional PWR systems, a two-phase (steam-water) mixture in the pressurizer receives hot-leg core outflow from the RPV and channels the flow into the steam generator unit(s). A pressurizer surge line and electrical heaters regulate the volumes of the two phases. One of the first modular PWRs, IRIS, used a design with an integrated pressurizer and steam generator. The pressurizer, in direct contact with the hot leg, generated sufficient pressure to direct flow into the RCPs. The RCPs then direct primary coolant to an annular steam generator. Like the IRIS design, integrated units modularize the primary circuit of a conventional pressurized water reactor into a single RPV [1]. Consequently, the increased height of the RPV provides housing volume for all reactor internals, instrumentation and CRDMs. This safety-by-design approach eliminates the need for HPSI pumps and thus, the possibility of pump failure, while also negating the occurrence of a total loss of feedwater [2]. The current study is based on the 800 MWth (>225 MWe) PWR-type SMR (WSMR) designed by Westinghouse Nuclear. Figure 1 shows a schematic of the flow paths in the WSMR. With integrated pressurizer designs, the hot leg flows are vertical unlike those with conventional PWRs. To sustain flow in the closed loop, a greater dynamic pressure is required for the coolant exiting the upper core. The increased height of the RPV is expected to channel core outflow towards the pressurizer, by creating a constriction – the ‘transition cone’, which reduces available flow area and directs flow into an extruded vertical conduit – the ‘hot leg riser’. The height of the hot leg riser is set equal to the height of the core barrel. Since the integral

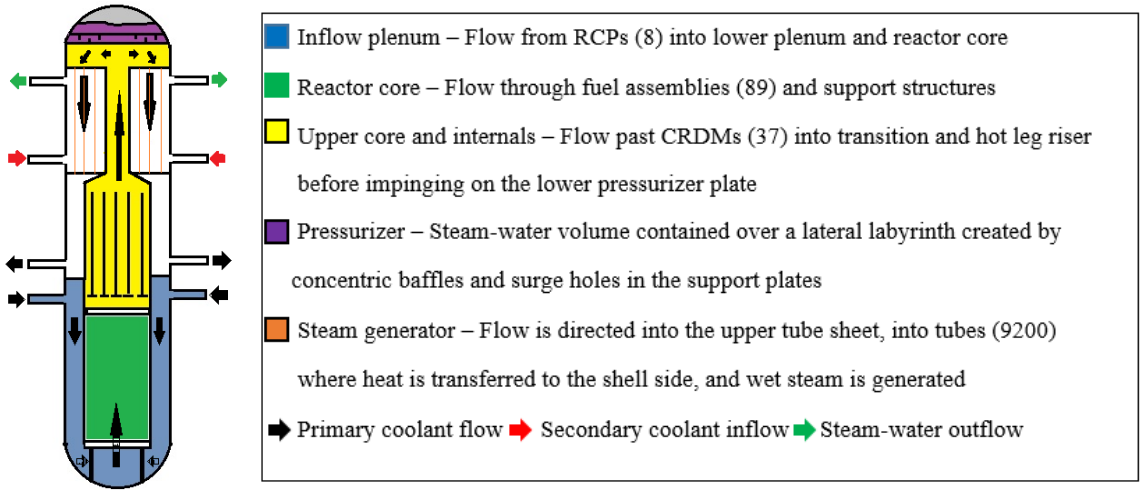

Figure 1. A schematic representation of primary and secondary flow paths in the WSMR.

steam generator is located as an annulus with respect to the hot leg riser, flow must reverse into the upper tube sheet of the steam generator. To achieve this, the pressurizer volume is fitted with a baffle plate with 12 peripheral surge holes to interact with the two-phase mixture. Figure 2 shows a 3D CAD model of the pressurizer used in this study.

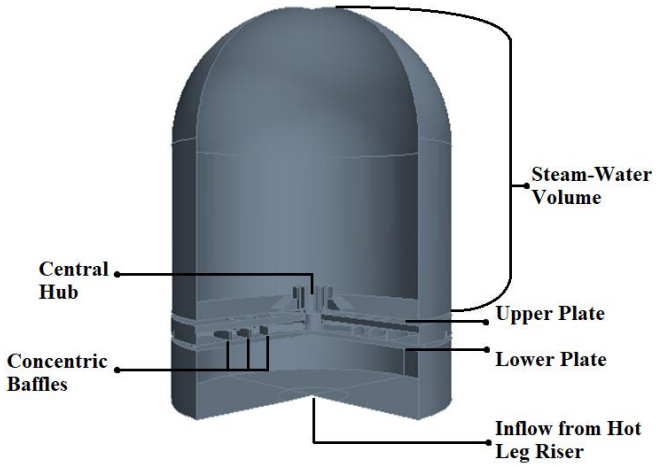

Figure 2. 3D CAD model of the integral pressurizer in the WSMR.

2. SIMILARITIES AND DIFFERENCES BETWEEN WSMR AND IRIS PRESSURIZER DESIGNS

The design of the WSMR pressurizer is based on the modularity of the IRIS pressurizer. However, from Figure 2 and published work by Carelli [3], it is apparent that significant differences exist in the pressurizer designs for the two reactors. In the WSMR, all CRDMS are located inside the RPV and the heater instrumentation is connected to the RPV support flange. By comparison, the IRIS pressurizer, has slots in the RPV dome for both instrumentation and the heaters. In the WSMR, surge orifices are located on the lower pressurizer plate, and the flow path to the central hub is via a tortuous path between the baffles. This path is expected to create a sufficient static pressure drop, reducing contact time and area between sub-cooled primary coolant and saturated water from the steam-water volume. The surge orifices in the IRIS pressurizer however, are located on the single insulated boundary and are located directly below the heaters so that the sub-cooled coolant rising into the sub-pressurizer plenum is directly exposed to the heater surfaces. The electric heaters in the WSMR pressurizer are horizontal and radially located around the RPV wall towards the bottom of the two-phase region, whereas, the heaters in the IRIS pressurizer are vertical and extend through the two-phase region. Lastly, the IRIS design is fitted with reactor coolant pumps (RCPs) to increase the dynamic pressure of the sub-cooled coolant at the top of the hot leg riser, before flow into the upper tube sheets of the steam generator units [4]. On the other hand, the WSMR is fitted with a transition cone and hot leg riser above the upper core support structures, reducing available flow area and increasing the average velocity leaving the upper core [5].

Accordingly, the only RCPs are at the outflow end of the lower tube sheet below the once-through steam generator unit.

The current study simulates turbulent flow in the computational model of the WSMR pressurizer using four RANS models with transient formulations. Based on their time-averaged hydrodynamics, a turbulence model is selected for further investigation of turbulent flow into the upper tube sheet and on the shell-side of the integral once-through steam generator.

3. COMPUTATIONAL DESIGN AND NUMERICAL METHODOLOGY

3.1. COMPUTATIONAL DESIGN OF THE WSMR PRESSURIZER

Table 1 lists the thermophysical properties of the primary coolant considered in both, stage 1 and stage 2 of simulations. All properties were evaluated at 607 K and 15.5 MPa based on outflow conditions from a prior simulation study [6].

Table 1. Thermophysical properties of the primary coolant.

Density	638.56 kg/m^3
Dynamic Viscosity	7.4278E-5 Pa-s
Specific Heat	7112.9 J/kg-K
Thermal Conductivity	0.4881 W/m-K
Turbulent Prandtl Number	0.9

3.1.1. Stage 1: Performance of RANS Turbulence Models. Stage 1 uses the top of the hot leg riser and the top of the upper tube sheet are respectively set as the domain inlet and outlet boundaries. The pressurizer is simulated in its entirety. Two parallel

pressurizer plates, separated by concentric baffles, alternately attached to the lower and upper plates separate the primary flow from the two-phase volume. The lower plate has 12 orifices along the circumference which provide access to the volume below the two-phase region, in between the baffles. The upper plate has a central hub where radial vertical baffles direct flow to central holes in the upper plate to interact with the steam-water volume. The computational model focuses on transient flow phenomena that occur during steady state operation i.e. 100% operating liquid level in the pressurizer. To further reduce the geometric complexity, the heaters are not modeled. Table 2 lists the operating and boundary conditions used in stage 1 of the simulation study.

Table 2. General initial and boundary conditions for stage 1 of simulations.

Operating Pressure	2250 psia
Inlet Velocity [5]	11.92 m/s
Steam Volume	19.435 m^3
Steam-Water Volumetric Ratio	~1.5:1
Gravity	[0, 0, -9.81] m/s^2

3.1.2. Stage 2: Simulation of T-H in the Pressurizer and Steam Generator. In the second stage, a sector of the steam generator is simulated such that the vertical boundaries of the sector form a pair of cyclic boundaries, set as ‘rotational periodic interfaces’ in the simulation. This reduces the cell count of the simulation domain while retaining complete geometric detail within the sector. In the first stage, the mesh is generated with emphasis on near-wall refinement suited to turbulence models resolving boundary layer flows. In the second stage, the mesh is generated with mesh refinement near the base of the upper tube sheet where primary coolant enters the tube-side of the

steam generator. Turbulent flow on both, the tube-side, and the shell-side is modeled with the selected turbulence model from section 4.1. whereas two-phase flow on the shell-side is modeled with the Volume of Fluid (VOF) model. All convective flows were solved with first order spatial accuracy. On the shell-side, the secondary coolant (H2O(l)) enters at a velocity of 5 m/s and a temperature of 500 K. Table 3 lists the thermophysical properties of the secondary coolant in the shell-side of the steam generator, evaluated at a mean secondary coolant temperature of 521.5 K and 5.5 MPa.

Table 3. Thermophysical properties of fluids in the steam generator.

	Secondary-Side ($H_2O_{(l)}$)	Secondary-Side ($H_2O_{(g)}$)
Density	803.22 kg/m^3	28.143 kg/m^3
Dynamic Viscosity	1.0733E-4 Pa-s	1.8283E-5 Pa-s
Specific Heat	4831.3 J/kg-K	4661.8 J/kg-K
Thermal Conductivity	0.62511 W/m-K	0.05716 W/m-K
Turbulent Prandtl Number	0.9	0.9
Saturation Enthalpy (T_{sat} = 543.3 K)	1186000 J/kg	2789600 J/kg

3.2. NUMERICAL METHODOLOGY

This sub-section elaborates on conservation equations and transient formulation of turbulence models used in the simulations. A primary difference in available turbulence models is the approach to model the Reynolds stress tensor and provide closure to the underlying equations.

3.2.1. Mass and Momentum Conservation Equations. In transient calculations, RANS turbulence models use ensemble averaged values of solution variables. Solution variables may be treated as a combination of fluctuating and mean components; when

substituted in the Navier-Stokes equations yield the following equations for mass and momentum conservation:

Mass conservation equation:

$$\frac{\partial \rho}{\partial t} + \nabla.(\rho \bar{\mathbf{v}}) = 0 \quad (1)$$

Momentum conservation equation:

$$\frac{\partial}{\partial t}(\rho \bar{\mathbf{v}}) + \nabla.(\rho \bar{\mathbf{v}} \times \bar{\mathbf{v}}) = -\nabla.\bar{p}\,\mathbf{I} + \nabla.(\mathbf{T} + \mathbf{T}_t) + \mathbf{f}_b \quad (2)$$

Reynolds stress tensor:

$$\mathrm{T}_t = -\rho \begin{pmatrix} \overline{u'\,u'} & \overline{u'\,v'} & \overline{u'\,w'} \\ \overline{v'\,u'} & \overline{v'\,v'} & \overline{v'\,w'} \\ \overline{w'\,u'} & \overline{w'\,v'} & \overline{w'\,w'} \end{pmatrix} \quad (3)$$

ρ	fluid density
$\bar{\boldsymbol{v}}$, $\bar{p}$	mean values of velocity, pressure
I	identity tensor
T	viscous stress tensor
$\mathbf{f}_b$	total of body forces on fluid volume
u', v', w'	fluctuating values of x, y, and z components of velocity

3.2.2. Realizable k-ε Model. The realizable k-ε model is a variant of the standard k-ε model, a two-equation model that solves for kinetic energy, *k,* and rate of energy dissipation, *ε*, to obtain the viscosity of turbulent eddies. The transport equations and associated constants have been incorporated into STAR-CCM+ after extensive validation in literature [7-8]. A primary improvement in the standard k-ε model were modifications to the equation representing the rate of energy dissipation, *ε*, and replacing coefficient, C_μ, as a function of mean turbulence parameters (*k, ε*) instead of a constant (~0.09), which enables realizability of normal stresses in turbulent flow to calculate the eddy

viscosity and has been validated with experiments on boundary layers. The new equation for ε is based on the dynamic mean-square fluctuation of vorticity [9].

3.2.3. SST k-ω Model. Based on the standard k-ε model, the standard k-ω model includes transport equations for kinetic energy, *k*, and dissipation per kinetic energy ω, to obtain the viscosity of turbulent eddies. The standard k-ω model has performed better than the standard k-ε model in resolving boundary layer flows under unfavorable pressure gradients but predictions are significantly affected by variation of ω in the bulk flow, and thus to inflow conditions. To circumvent this limitation, the SST k-ω model uses an additional cross-diffusion term containing $(\nabla k.\nabla\omega)$ which mitigates the effects of variation in ω away from the wall, while turbulent boundary layer flows are effectively solved for [10].

3.2.4. Reynolds Stress Turbulence Model (RSM). Reynolds stress models such as RSM can precisely predict complex flows by inherently considering anisotropy, rotation and adverse strain rates in turbulent flow regimes. A Favre averaging of the product of RANS equations and fluctuating solution variables results only in modeling of the pressure strain, diffusion and dissipation terms [11]. The Linear Pressure-Strain model is used in this study which can also well resolve wall dominated flows in low $y+$ regions.

3.2.5. Spalart-Allmaras Model. This one-equation model calculates the diffusivity, $\tilde{\vartheta}$, to obtain the viscosity of turbulent eddies. As a low-Reynolds number model, it was chosen for this study because of flow reversal expected upon impact of inflow at the lower pressurizer plate. During this reversal, an abrupt change in axial velocity is expected due to 180^0 change in flow path, which would suggest the formation

of thick, turbulent boundary layers, low-Reynolds number flows, and marginal separation in the bulk flow. The Spalart-Allmaras model has been validated in accurate resolution of viscous sublayers, mild flow separation, and suited for unstructured solvers [12].

4. RESULTS

4.1. STAGE 1: PERFORMANCE OF RANS TURBULENCEMODELS

To determine the physical time for simulations, a passive scalar was used to track the residence time and was estimated at 2.4 s. Then, a simulation with each turbulence model was run for 12 residence times and a time-averaged velocity profile was obtained. A comparison of time-averaged velocity magnitudes is provided in Figure 3.

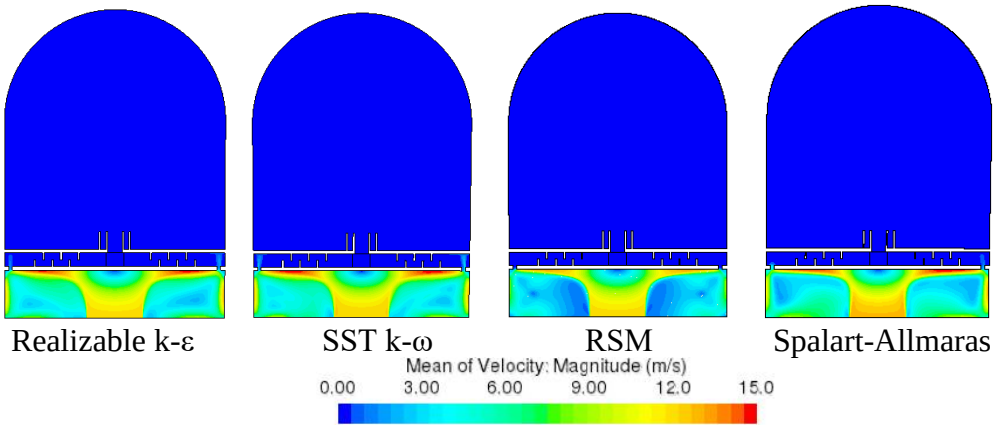

Figure 3. Time-averaged velocity profiles reported by the RANS turbulence models.

While the qualitative predictions of the turbulence models are similar, the RSM model predicts some salient differences. Firstly, there is little lateral diffusion in the bulk flow near the inlet as may be inferred from Figure 3. The clearance between the inlet and

the lower pressurizer plate is approximately 1 m, through which an inlet velocity of 11.92 m/s suggests primarily vertical flow. Inflow faces a significant increase in flow area which would suggest lateral dissipation, but only upon impingement at the lower pressurizer plate. Secondly, the RSM model is able to predict significantly smaller IRZs as may be expected during flow reversal and mild separation. This phenomenon is also indicative of transience in the formation of vortices and their breakup in rotational flow. The Spalart-Allmaras model next best predicts the above mentioned phenomena with a more diffuse profile, but like the realizable k-ε and SST k-ω models, is neither able to capture the separation of IRZs nor indicate rotational flow like the RSM model. This may be attributed to the RSM model accounting for contributions from additional shear stress terms which as apparent, create a significant difference in the accuracy of flow

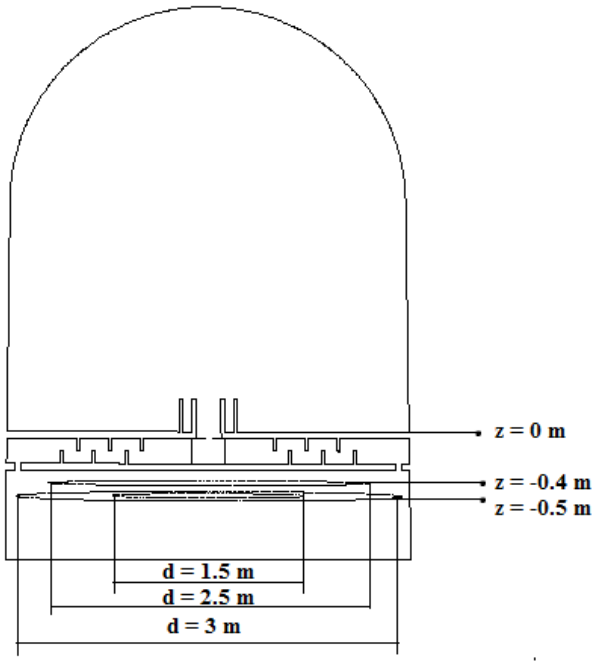

Figure 4. Sampling locations set up to assess lateral variations in velocity.

resolution. This additional contribution alters the local flow field resulting in a thinner layer of high velocity flow upon impingement on the lower pressurizer plate, as observed in Figure 3. However, these inferences are based on axial flow representations. In order to assess lateral variation in flow, three circular probes were set up at the locations shown in Figure 4. The axial and diametric specifications have additionally been indicated.

In Figure 5, velocity vectors are plotted at the locations listed in Figure 4; from top to bottom, the locations are (z, d) = (-0.5, 1.5), (-0.4, 2.5), and (-0.5, 3), with all dimensions in meters. Notable in Figure 5, is the relative uniformity in velocity magnitude and vector direction predicted by the RSM model at all three sampling locations. This corroborates with the inferences from Figure 4, and the Spalart-Allmaras model provides qualitative agreement with predictions of the RSM model, but with significant difference in local

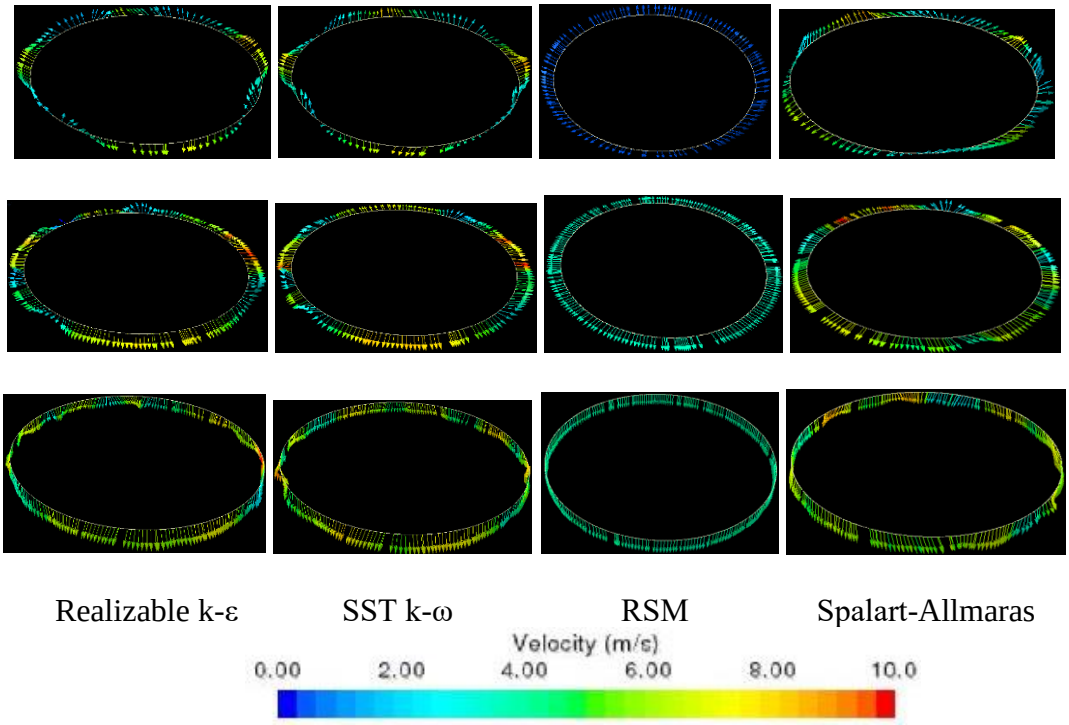

Figure 5. Vector plots of velocity magnitude predicted by stage 1 of simulations.

velocity magnitudes. The third sampling location is within 0.1 m of the wall, and impinging flow at the lower pressurizer plate is observed to laterally dissipate and descent into the upper tube sheet of the steam generator. In a cylindrical domain such as the pressurizer, the flowpath is relatively symmetric and flow descending along the pressurizer walls is dominated by axial flow. Based on these observations, the RSM model was best suited for stage 2 of simulations.

4.2. STAGE 2: SIMULATION OF FLOW AND HEAT TRANSFER IN THE INTEGRAL STEAM GENERATOR

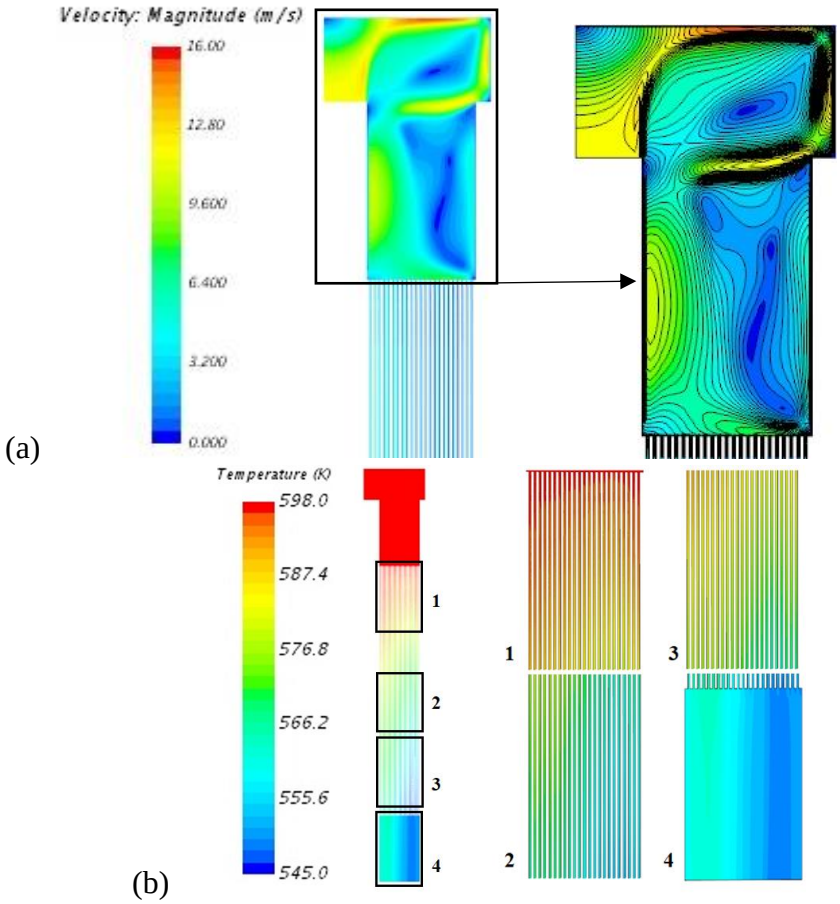

Figure 6. Profiles of (a) velocity and (b) temperature of the primary coolant on the tube side of the integral steam generator.

This stage combines the pressurizer domain with the tube side of the integral steam generator, and simulates heat transfer and hydrodynamics on the shell-side. Figure 6 shows a representation of velocity on an axial cross-section of the tube-side and the distribution of temperature through the tubes. As the primary coolant descends the tubes, the temperature of the fluid decreases owing to heat transfer to the shell-side. On the shell side, the temperature of the subcooled water rises to saturation where steam is formed and a steam-water mixture flows out of the steam generator. The distribution of the steam-water mixture across the axial and lateral cross-section planes is presented in Figure 7, with streamlines of mixture velocity. It may be inferred that the density difference between steam and water allows the steam to rise to the upper surface of the shell side. Streamlines of mixture velocity and volume fraction of steam between the inlet and outlet show an increase in the volume fraction of steam along the height of the tubes, concurrent with a decrease in mixture velocity. The outlet-averaged volume fraction of steam was reported to be 0.58. The design target for the integral steam generator was 0.6.

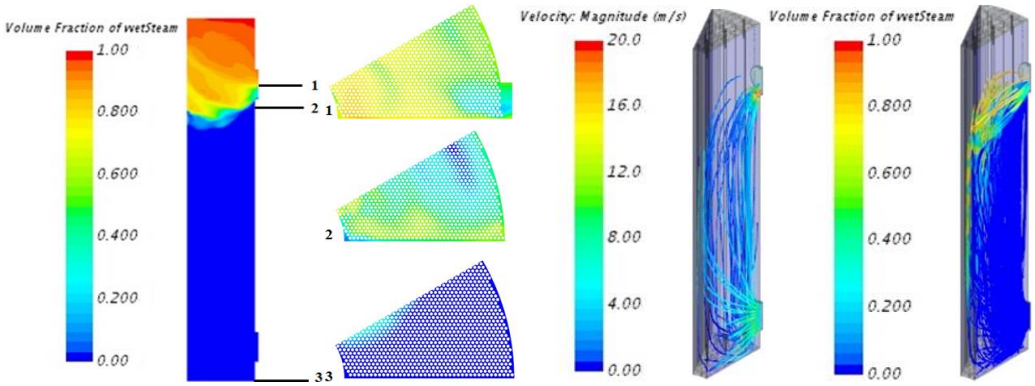

(a) (b)

Figure 7. (a) Axial and lateral cross-section profiles of steam volume fraction (b) streamlines of velocity and steam volume fraction between the inlet and outlet of the shell side.

5. CONCLUSIONS

Turbulent hydrodynamics in the integral pressurizer and steam generator units of a 800 MWth PWR-type small modular nuclear reactor were simulated in a two stage study. In the first stage, the realizable k-ε, SST k-ω, RSM and Spalart-Allmaras models were used to predict turbulent flow profiles below the lower surface of the pressurizer plate. Of the four models, the RSM model was able to predict rotational structures in the interior flow and reported relative uniformity in the lateral flow profiles at radial sampling locations in the volume of flow reversal. In the second stage of the study, the RSM model was used to simulate turbulent flow out of the hot leg riser into the tube side of the integral steam generator. The RSM model was also used to simulate turbulent flow of the secondary coolant into the shell side of the steam generator, and steam-water flow was modeled using the VOF multiphase flow model. Temperature and velocity profiles were presented from both, tube and shell sides. Streamlines of velocity on the shell side were compared with streamlines of steam volume fraction, and the generation of steam was consistent with a decrease in velocity. The steam-water mixture exiting the shell side was averaged at 0.58, with a design target of 0.6.

ACKNOWLEDGEMENTS

The authors would like to thank Westinghouse Electric Company LLC. for their guidance in the study and the Small Modular Reactor Education & Research Consortium for their financial support. The authors would also like to thank the Oak Ridge

Computing Facility, Oak Ridge National Laboratory for providing access to computational resources for this study.

REFERENCES

1. Collado, J. M. Design of the Reactor Pressure Vessel and Internals of the IRIS Integrated Nuclear System. https://www.nrc.gov/docs/ML0336/ML033600078.pdf; date last accessed: April 22, 2018.

2. Carelli, M. D. IRIS Advanced Features and Status. A presentation to Oak Ridge National Laboratory, Oak Ridge, TN. December 20, 2005.

3. Carelli, M.D. et. al. 2003. The Design and Safety Features of the IRIS Reactor. 11th International Conference on Nuclear Engineering, Tokyo, Japan. ICONE11-36564.

4. Barroso, A.C.O. et. al., 2003. IRIS Pressurizer Design. Proceedings of ICAPP '03, Cordoba, Spain, May 4-7, 2003, Paper 3227.

5. Small Modular Reactor | Westinghouse Nuclear. 2018. http://www.westinghousenuclear.com/New-Plants/Small-Modular-Reactor. Date last accessed: April 22, 2018.

6. Rao, V. M. and Smith, J. D. 2018. CFD Analysis of Turbulent Forced Convection in the Reactor Core and Flow Past Internal Structures in a PWR-Type Small Modular Nuclear Reactor. Article under peer review, Annals of Nuclear Energy, submitted April 2018.

7. Jones, W. B., and Launder, P. E. The Calculation of Low-Reynolds-Number Phenomena with a Two-Equation Model of Turbulence. International Journal of Heat and Mass Transfer. 1973. 16 (6), pp. 1119-1130.

8. Launder, B. E., and Sharma, B. T. Application of the energy dissipation model of turbulence to the calculation of flow near a spinning disc. Lett. Heat and Mass Transfer 1. 1974. pp. 131–138.

9. Shih, T-H., Liou, W. W., Shabbir, A., Yang, Z., and Zhu, J. A New k-ε Eddy Viscosity Model for High Reynolds Number Turbulent Flows-Model Development and Validation. NASA Technical Memorandum 106721 ICOMP-94-21; CMOTT-94-6. August 1994.

10. Menter, F. R. Two-Equation Eddy-Viscosity Turbulence Models for Engineering Applications. AIAA Journal. 32 (8) August 1994.

11. Versteeg, H., and Malalasekra, W. An Introduction to Computational Fluid Dynamics: The Finite Volume Method. Pearson Education Ltd. Second Edition. 2007. pp. 94-99.

12. Spalart, P. R. Strategies for Turbulence Modeling and Simulations. International Journal of Heat and Fluid Flow. 2000. 21, pp. 252-263.

SECTION

2. CONCLUSION

A computational model of a PWR-type SMR was developed based on existing designs of the AP 1000 and SMR (WSMR) by Westinghouse Nuclear. The reactor core for the SMR was set to output 800 MW, as with the WSMR. Novel additions to the WSMR incorporated in the computational SMR design included a pressurizer unit, an annular once-through steam generator unit, and CRDMs entirely contained within the RPV. Using this new design, the objective was to resolve turbulent flow and conjugate heat transfer on the primary side and quantify heat available from the steam-water mixture on the secondary side to generate electricity. To accomplish this, the computational design was divided into four simulation domains – the lower plenum, the reactor core and upper internals, the pressurizer, and the steam generator. In each domain, commercial CFD package, STAR-CCM+, was used to simulate desired phenomena and quantify metrics for numerical verification.

In the lower plenum, turbulent flow was resolved on a preliminary mesh using four RANS turbulence models to assess their performance, among which, the RST model was found to be most suitable, then used to simulate time-averaged turbulent flow on a fine mesh and compared with time-averaged predictions of the LES model. The RST model provided satisfactory agreement with time-averaged hydrodynamic predictions of the LES model. The LES model was also successful in capturing the range of spatial frequencies that describe the inertial sub-range of turbulent kinetic energy in the lower

plenum. Outflow conditions from the lower plenum (through the lower core plate) were used as inflow conditions for the reactor core and upper internals domain.

The reactor core was designed to consist of 89 17x17 fuel assemblies as per the WSMR design. From a single 17x17 fuel assembly, a bottom nozzle was designed in its entirety through which flow was simulated using the realizable k-ε model. A representative volume of the fuel assembly reduced to a 3x3 array and spacer grid volumes contained within, was then simulated in two stages, to capture thermal-hydraulic phenomena. The first stage simulated the entire length of the representative volume, while the second stage simulate segments of the representative volume along the active height of the 3x3 array. Both approaches showed good agreement in thermal predictions, with an averaged core outlet temperature of 605 K - 609 K. Then, turbulent flow through the top nozzles of all 89 fuel assemblies, CRDMs, TPAs, RCCAs, upper core and support plates, transition cone, and hot leg riser was simulated to capture core outflow phenomena.

Turbulent flow through the pressurizer was simulated, as with the lower plenum, using four RANS turbulence models – the realizable k-ε model, the SST k-ω model, the RST model, and the Spalart-Allmaras model. In the flow volume, a 180^0 flow path reversal was expected to create mild flow separation, lateral vortices, and rotational flow. After assessing the performance of the turbulence models, the RST model was selected as most suitable in predicting turbulent flow and assigned to simulate downstream turbulent flow through the tube side of the once-through steam generator. The RST model was also used to simulate turbulent flow on the shell side of the steam generator, accompanied by the VOF Boiling model to simulate multiphase interactions and wall boiling.

BIBLIOGRAPHY

1. Roege, P. E. et al. Metrics for Energy Resilience. Energy Policy, 2014, vol. 72, issue C, pp. 249-256.

2. U.S. Department of Energy. Quadrennial Technology Review, Chapter 4: Advancing Clean Power Technologies. 2015.

3. Antkowiak, M. et al. Summary Report of the INL-JISEA Workshop on Nuclear Hybrid Energy Systems. Joint Institute for Strategic Energy Analysis. 2012.

4. Ingersoll, D. T. et al. Can Nuclear Power and Renewables be Friends? Proceedings of ICAPP 2015. May 03-06, 2015 – Nice (France). Paper 15555.

5. Garcia, H. E. et al. Nuclear Hybrid Energy Systems – Regional Studies: West Texas & Northeastern Arizona. 2015. Idaho National Laboratory. INL/EXT-15-34503. Revision 0.

6. Bragg-Sitton, S. et al. Integrated Nuclear-Renewable Energy Systems: Foundational Workshop Report. National Renewable Energy Laboratory. INL/EXT-14-32857. Rev. 1. NREL/TP-6A20-62778.

7. Buchheit, K. L. et al. Techno-Economic Analysis of a Sustainable Coal, Wind, and Nuclear Hybrid Energy System. 2016. Energy Fuels. 30 (12), pp. 10721-10729.

8. NuScale Power, LLC. www.nuscalepower.com. Date accessed: July 17, 2017.

9. Westinghouse Electric Company, LLC. http://www.westinghousenuclear.com/New-Plants/Small-Modular-Reactor. Date accessed: July 17, 2017.

10. Advanced Reactor Concepts, LLC. http://www.arcnuclear.com/arc-100-reactor. Date accessed: July 17, 2017.

11. AREVA Inc. http://us.areva.com/EN/home-3225/areva-inc-areva-htgr.html. Date accessed: July 17, 2017.

12. X Energy, LLC. http://www.x-energy.com/copy-of-technology. Date accessed: July 17, 2017.

13. Terrestrial Energy Inc. http://www.terrestrialenergy.com. Date accessed: July 17, 2017.

VITA

Vivek Murlidhar Rao was born in Bangalore, KA India, and grew up in Mumbai, MH India, where he completed K-12 study. In 2006, Mr. Rao relocated to Bangalore to complete a university degree (Bachelor of Engineering) in chemical engineering under the purview of Visvesvaraya Technological University. Upon securing a bachelor's degree in 2010, Mr. Rao sought to extend academic study in the United States of America at the Missouri University of Science & Technology, Rolla MO, with a master's degree in chemical engineering. During this time, Vivek worked under the combined supervision of Dr. Muthanna H. Al-Dahhan and Dr. Carlos H. Castano to further a novel technique in synthesis and characterization of transition-metal nanoparticles using gamma-radiation and femtosecond laser ablation techniques, unconventional to the field. Towards the end of his master's program, Mr. Rao took interest in renewable and hybrid energy systems research conducted by Joseph D. Smith, PhD., the Laufer Endowed Energy Chair in the Department of Chemical and Biochemical Engineering. Mr. Rao was offered for his doctoral dissertation, a challenging project that subjected the inter-disciplinary design process of a modular, nuclear fission reactor through verification and validation requirements. Since then, Mr. Rao has also served as instructor for several graduate and undergraduate courses taught by the departments of chemical engineering, chemistry, and nuclear engineering. Mr. Rao obtained his PhD in chemical engineering from Missouri University of Science & Technology in July 2018.